Development of a Compliant Dashpot Model with Nonlinear and Linear Behaviors for the Contact of Multibody Systems

Gengxiang Wang[1,2] (wanggengxiang@pku.edu.cn)
Daolin Ma[3] (daolinma@sjtu.edu.cn)
Caishan Liu[2] (liucs@pku.edu.cn)
Yang Liu[4] (y.liu2@exeter.ac.uk)

1. School of Mechanical and Electrical Engineering, Xi'an University of Architecture and Technology, Xi'an 710055, Shaanxi, China
2. State Key Laboratory for Turbulence and Complex Systems, College of Engineering, Peking University, Beijing, 100871, China
3. School of Naval Architecture, Ocean and Civil Engineering, Shanghai Jiaotong University, 200240 Shanghai, China
4. College of Engineering, Mathematics and Physical Sciences, University of Exeter, Exeter, EX4 4QF, UK

ABSTRACT

A comprehensive dashpot model with hysteresis damping factors that can provide a convenient calculation approach for the elastoplastic impact behavior in multibody systems is studied in this paper. At the beginning of contact, the nonlinear hysteresis damping factor in the elastic phase is derived by approximately solving a nonlinear vibration system. When the impact happens under relatively high speed and large load, the elastoplastic deformation is inevitable, and the Hertz contact stiffness cannot represent the actual contact stiffness. In order to correctly describe the contact stiffness in the elastoplastic or plastic phase. In this model, a static elastoplastic contact model is adopted to calculate the contact stiffness by approximately linearizing the relationship between load and deformation. When the contact comes into the elastoplastic phase, the impact behavior can be treated as a linear vibration system, and the linear hysteresis damping factor can also be obtained from this linear system. The energy dissipation in different contact phases can be described by a nonlinear and a linear hysteresis damping factor. Such a nonlinear hysteresis damping factor can make up for the deficiency of the static elastoplastic contact model in describing the energy dissipation in the elastic contact phase. Simulation results show that the proposed dashpot model is more harmonious with the static elastoplastic contact model compared to the existing dashpot models. A slider-crank mechanism with a clearance joint and a Hopkinson incident bar are exemplified in the present work by using experimental data to validate the effectiveness of the proposed dashpot model.

Keywords: Elastoplastic deformation; Hysteresis damping factor; Contact stiffness; Vibration system

1. Introduction

Contact events are ubiquitous in multibody systems [1][2,3]. In general, the contact deformation caused by the collision includes elastic and plastic deformations [4]. The elastic deformation always happens at the beginning of a contact behavior [5][6], while the plastic deformation is prone to the contact materials with a large Young's modulus and a small yield stress, especially with a high initial impact velocity or a high load [7–11]. When indentation surpasses the critical elastic threshold, plastic and elastic deformations occur simultaneously. Modeling elastic and plastic contact behaviors [12], distinguishing two different contact deformation phases, and developing an appropriate contact force model are crucial questions in contact mechanics of both macro and micro scales [13–15]. Critical elastic deformation was used to define the inception of plastic deformation in contact processing [16], which was calculated based on Hertz theory associated with the Mises yield criterion [17]. It is known that, when contact deformation occurs within the limitation of elastic contact deformation [18], the nonlinear contact behavior is governed by the Hertz contact law [5]. However, the question is, when the contact deformation surpasses the critical contact deformation, what kinds of contact model can be employed to predict the dynamic process of the plastic collision event? Apparently, the existing contact force models with hysteresis damping factor [5,19–25] developed using the Hertz contact law cannot be used to evaluate the contact force in the elastoplastic or the plastic deformation phase [8,9,12,16,17,26–28]. In addition, existing static contact force models [8,28,29] that mainly focus on the relation between loading force and contact deformation are not convenient to be used for evaluating the dynamic contact process [30], since they do not have the hysteresis damping factors [12,31–34].

For the static elastoplastic contact models, many scholars concentrated on developing the constitutive relation between the contact bodies when plastic deformation happens [35,36]. Chang, Etsion and Bogy [37] (CEB) attempted to develop an impact model based on the statistics model between rough surfaces [38]. This model is referred as the CEB model, including the elastic and full plastic contact phases, which explains the plastic deformation phenomenon using the yield coefficient that is a function of Poisson's ratio. Nevertheless, this model suffers from a discontinuity between the elastic and the plastic phase [4]. In Johnson's model [39], it provided a simple and convenient relation between restoring force and indentation, and proved that the elastoplastic phase is a very long process and conspicuous phenomenon. Zhao, Maietta, and Chang (ZMC model) [12] presented an elastic-plastic asperity microcontact model applied between two nominally flat surfaces [40]. In the elastoplastic phase, the relationship between contact pressure and deformation was expressed using the logarithmic function. The interference of the contact area was modeled by a fourth-order polynomial function. The results showed that the ZMC model is more accurate in describing the contact of rough surfaces than the CEB model. In order to obtain the continuous static contact force model, Jackson and Green (JG model) [8,16] developed the best fit polynomial relationships for describing the function relation between the interference forces. Stronge [41] employed the approximate approach to study the mixed elastic-plastic and full plastic regimes. Thornton [42] proposed a simplified theoretical model for the normal contact interaction between two elastic-full plastic spheres based on the discrete element code. Du and Wang [43] proposed a theoretical model of elastoplastic impact for two spheres, including the elastic, elastoplastic, and full plastic phases, and used finite element model (FEM) to verify its correctness. Zhang and Vu-Quoc [44] proposed an elastoplastic collision model when modeling the relationship between the coefficient of restitution (CoR) and initial impact velocity without friction [45]. Mesarovic and Fleck [46] found that the contact behaviors were entirely different in the fully plastic phase for a sphere pressed by a rigid flat and for a half-space indented by a rigid sphere. Although FEM can obtain an accurate plastic contact force model,

it is inefficient for contact events with complex geometric shapes, because a tremendous amount of meshing is required [10,47]. In our recent studies, Ma and Liu [4] developed an analytical approximation model for the elastoplastic phase inspired by Johnson's simplified spherical expansion model [32]. A complete static contact force model without discontinuity was derived by smoothly connecting the critical elastic and plastic contact conditions [8][29], which successfully described the relationship between the contact force and deformation for the elastic, elastoplastic, and plastic contact phases in a smooth manner [48]. More importantly, the Ma-Liu model predicted the correct elastoplastic contact stiffness and CoR and has been validated by experiment. Therefore, the Ma-Liu model [4] will be considered as a fundamental model in this work for developing a comprehensive dashpot model with hysteresis damping factors. However, it is worth noting that, for all existing static elastoplastic contact models, the relationship between load and deformation approximates linear [49] when the contact comes into the elastoplastic or the plastic phase [38].

Around 30 types of dashpot models with hysteresis damping factors [13] were formulated based on the Hertz contact law [50], which was used to depict the elastic contact event from a dynamic point of view [51]. The main goal of the available dashpot models [52,53] is to continually enhance energy dissipation accuracy by improving the hysteresis damping factors [34,54]. These models do not care about the contact stiffness in the different contact deformation phases [55], which do not reflect the plastic deformation [51]. That is mainly because the existing contact force models with hysteresis damping factors [15] were developed within the elastic deformation scope [5,19–25]. They cannot be used to explain the elastoplastic or the plastic contact behaviors [33]. Therefore, the proposed dashpot model can depict different contact stiffness coefficients for all the contact deformation phases and establish the coupling relation between the contact force, contact velocity, and contact deformation.

Since the hysteresis damping factor is usually considered as a function of CoR [21–24,51,56–61], another issue is how to evaluate the CoR in different contact phases. The most common coefficient is Newton's CoR [8,32] that is equal to the ratio of impact velocities between before and after the contact. In addition, the CoR can be evaluated using the impulse-momentum or strain energy and kinetic energy during impact [19,20,25,26,58,62]. In general, when the contact happens within the elastic scope, the CoR is equal to 1 in the static contact force model [8,9], indicating that there is no energy dissipated in the elastic phase [45]. When the elastoplastic or the plastic deformation occurs, the CoR is smaller than 1 [4,54], which depicts the energy dissipation caused by the plastic deformation [8,11,42,63–65]. However, in the dashpot models, the hysteresis damping factor represents energy dissipation caused by the elastic wave propagation [61]. In fact, the elastic wave propagation[66], including compressional wave, shear wave, and Rayleigh wave, also dissipates the energy even in the elastic phase [32]. In order to exhibit the energy dissipation in different contact phases, the energy dissipation caused by elastic wave propagation is considered by a nonlinear hysteresis damping factor. On the contrary, the dissipated energy in the elastoplastic or the plastic phase can be estimated by a linear hysteresis damping factor.

1.1. Limitations of the models in the literature

In summary, the following limitations persist for the existing contact force models, including the dynamic dashpot and static contact force models:

(1) The static elastoplastic contact models primarily concentrated on modeling the relationship between contact deformation and loading force [1,12,16,32,36,64,65]. They are prone to be disturbed by the integrate error because the entire contact behavior only depends on the contact deformation and cannot directly obtain the coupling relationship between the contact force and

contact velocity due to lacking the damping factor. However, the existing dashpot models are only concerned with the elastic contact behavior. Although they can predict the entire dynamic contact process [19,20,22,23,57,59], they cannot accurately estimate the elastoplastic contact event as Hertz contact stiffness is not consistent with the actual contact stiffness in the elastoplastic phases [50].

(2) Although the static elastoplastic contact models can calculate the dynamic impact process of multibody systems, the compression and recovery phases must be distinguished in the simulation process [67,68]. Moreover, the maximum and residual contact deformations must be identified and saved in each collision for the following impact behavior. This is mainly due to the fact that the static elastoplastic model has a different path in the loading phase from the unloading phase [67]. This characteristic makes the calculation process of the impact behavior complicated. On the contrary, the dashpot models do not need to identify the compression and recovery phases since the whole contact process follows the same formulation [14,69,70], which simplifies the calculation process significantly for the elastoplastic contact behavior. That is why we need to develop the dashpot model suited for the elastoplastic impact event.

(3) The CoR in dashpot models is usually determined based on the experience or the experimental data before simulating the contact dynamics [8,17,42,46,71]. However, performing experiments to determine the CoR value costs too much and is not universal [28]. Utilizing the experience to confirm the CoR value results in an inaccurate solution [9]. Therefore, how to determine the CoR is still a troubling issue for the existing dashpot models. Although the static contact models can use the strain energies before and after the contact to calculate the CoR [11,32,33,47,71], they always ignore the energy dissipation caused by the seismic waves in the elastic contact phase, so they were rarely used in the dynamic prediction of contact event.

1.2. Main Contributions

The present work aims to develop a comprehensive dashpot model with hysteresis damping factors and elastoplastic deformation. Its main contributions can be summarized as follows:

(1) In order to accurately describe the impact behavior and energy dissipation, a complete contact process is divided into two different contact phases [67], including the pure elastic and elastoplastic phases. The impact behavior is treated as a combination system that consists of a nonlinear system in the elastic phase and a linear system in the elastoplastic phase. The nonlinear and linear hysteresis damping factors can be obtained by solving the corresponding vibration systems. A novel dashpot model in the elastic phase is proposed by using the Hertz contact stiffness coefficient and a nonlinear hysteresis damping factor [68]. When the elastoplastic deformation is activated, another new dashpot model is formulated by the linearized contact stiffness coefficient and a linear hysteresis damping factor. Therefore, a comprehensive dashpot model is established by a nonlinear dashpot model in the elastic phase and a linear dashpot model in the elastoplastic phase. Compared to the static elastoplastic contact model, the new dashpot model inherits the merit of the existing dashpot models to simplify the calculation process of the elastoplastic impact event in multibody systems, especially for the multi-collision and multi-compression behaviors.

(2) The CoR is no longer determined by experiences or experiments [4]. When the contact behavior is within the elastic phase, the CoR can be calculated directly according to the dissipated energy caused by the seismic waves. When the contact behavior is in the elastoplastic and plastic contact phases, the CoR can be identified using the static elastoplastic contact model [4,27,64,65,72,73].

1.3. Structure of this investigation

The remaining of this paper can be organized as follows: In Section 2, a static elastoplastic contact model developed by Ma and Liu is introduced in detail. The nonlinear and linear hysteresis damping factors are developed, and the new dashpot model is proposed in Section 3. The calculation of the CoR in the dashpot model is introduced in Section 4. In Section 5, the spherical joint with clearance is taken as an example to analyze the dynamic performances of the new dashpot model. In Section 6, the slider-crank mechanism with clearance joint and Hopkinson incident bar are taken as numerical examples to validate and understand the effect of elastoplastic deformation on the dynamic responses of a multibody system. The conclusions are summarized in Section 7.

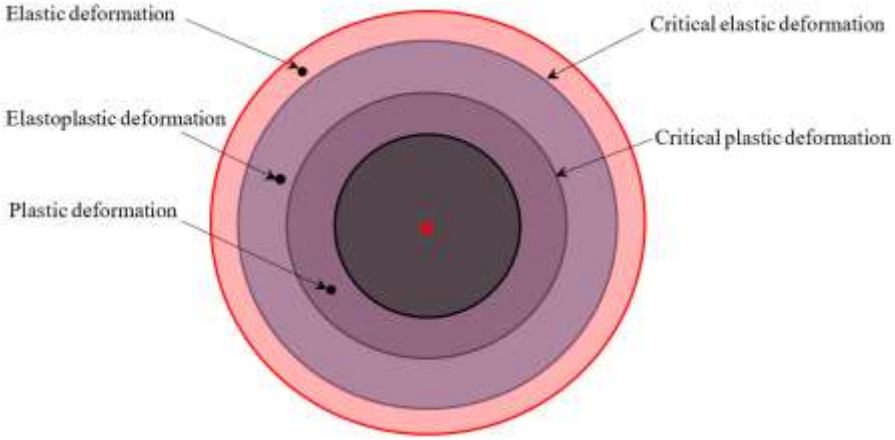

Fig.1 Contact body with different contact deformation phases

2. Static elastoplastic contact model (Ma-Liu model)

A contact body is depicted as the deformation area, as shown in Fig.1, wherein the deformation area embraces the elastic, elastoplastic, and plastic deformation. Plastic deformation is inevitable under high impact velocity or high load in the contact event. The loading and unloading process of the Ma-Liu model can be seen in Fig.2.

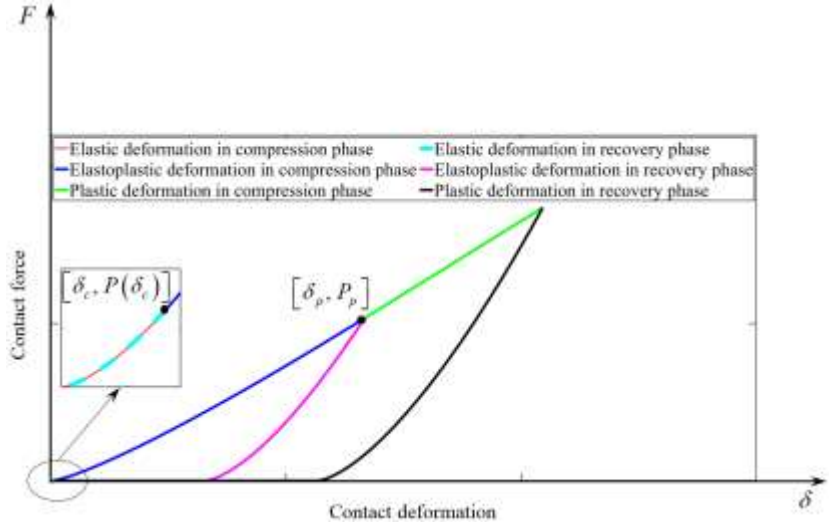

Fig.2 Relationship between the force and deformation

The static elastoplastic contact model can be obtained by a quasi-static compression experiment [7]. In Fig.2, the loading path is the same as the unloading path in the elastic phase that exhibits the nonlinear feature. However, once the deformation exceeds the critical elastic deformation, the contact

behavior comes into the elastoplastic or plastic phase. Significantly, the relationship between the force and deformation in the elastoplastic or plastic phase can be approximately treated as linear [67]. These contact characteristics of the Ma-Liu model provide the rational assumptions and theoretical foundation for developing the new complaint contact model with damping factors in the entire contact process.

2.1. Loading path

The loading path includes the elastic, elastoplastic and plastic compression phases, which is expressed as

$$P(\delta)=\begin{cases}\dfrac{4}{3}ER^{\frac{1}{2}}\delta^{\frac{3}{2}} & \delta<\delta_c\\ \delta\left(c_1+c_2\ln\dfrac{\delta}{\delta_c}\right)+c_3 & \delta_c\le\delta<\delta_p\\ P_p+k_1\left(\delta-\delta_p\right) & \delta\ge\delta_p\end{cases} \tag{1}$$

where $R=\dfrac{R_1R_2}{R_1\pm R_2}$, $\dfrac{1}{E}=\dfrac{1-\nu_1^2}{E_1}+\dfrac{1-\nu_2^2}{E_2}$, E is the composite Young's modulus, E_1 and E_2 are Young's modulus of the contact material, R_1 and R_2 are the radius of curvature of the contact bodies, ν_1 and ν_2 are the Poisson ratio of the contact bodies. The Hertz contact stiffness coefficient is expressed as $K_e=4ER^{\frac{1}{2}}/3$. The critical elastic deformation is written as $\delta_c=\dfrac{\pi^2R}{4E^2}p_y^2$, $p_y=1.61\sigma_y$, σ_y is the yield stress. $c_1=\dfrac{p_y\left(1+\ln\left(\varepsilon^2/2\right)\right)-2\psi\sigma_y}{\ln\left(\varepsilon^2/2\right)}\pi R$, $c_2=\dfrac{2\psi\sigma_y-p_y}{\ln\left(\varepsilon^2/2\right)}\pi R$, $c_3=P_c-c_1\delta_c$, $P_c\left(\delta_c\right)=\pi^3R^2p_y^3/6E^2$, ψ is the dimensionless parameter that corresponds to a ratio between the Brinell hardness and the yielding strength of the material, which is in the range from 2.6 to 3.0 [4]. ε is the dimensionless parameter that corresponds to a geometric relationship when the pressure on the contact surface approximately approaches uniformity, its value is within the scope from 13 to 20 [4]. The critical plastic deformation is expressed as $\delta_p=\varepsilon^2\delta_c/2$, $P_p=\delta_p\left(c_1+c_2\ln\left(\varepsilon^2/2\right)\right)+c_3$, $k_1=2\pi R\psi\sigma_y$.

The stored energy in the loading process can be expressed as

$$U_c(\delta)=\int_0^{\delta_{\max}}P(\delta)d\delta\begin{cases}\dfrac{8}{15}ER^{\frac{1}{2}}\delta_{\max}^{\frac{5}{2}} & \delta_{\max}<\delta_c\\ \dfrac{8}{15}ER^{\frac{1}{2}}\delta_c^{\frac{5}{2}}+\left(\dfrac{1}{2}c_1-\dfrac{1}{4}c_2\right)\left(\delta_{\max}^2-\delta_c^{\,2}\right)\\ +\dfrac{1}{2}c_2\delta_{\max}^2\ln\dfrac{\delta_{\max}}{\delta_c}+c_3\left(\delta_{\max}-\delta_c\right) & \delta_c\le\delta_{\max}<\delta_p\\ \dfrac{8}{15}ER^{\frac{1}{2}}\delta_c^{\frac{5}{2}}+\left(\dfrac{1}{2}c_1-\dfrac{1}{4}c_2\right)\left(\delta_p^2-\delta_c^{\,2}\right)+\dfrac{1}{2}c_2\delta_p^2\ln\dfrac{\delta_p}{\delta_c}\\ +c_3\left(\delta_p-\delta_c\right)+P_p\left(\delta_{\max}-\delta_p\right)+\dfrac{1}{2}k_1\left(\delta_{\max}-\delta_p\right)^2 & \delta_{\max}\ge\delta_p\end{cases} \tag{2}$$

where $\delta_{\max}$ is the maximum contact deformation.

2.2. Unloading path

When the contact deformation achieves the maximum contact deformation, the relative contact velocity becomes zero, the rebound or restitution phase will be started. Only elastic deformation occurs in this phase, which complies with the Hertz law. The contact force at this phase can be expressed as

$$P(\delta)=\begin{cases}\dfrac{4}{3}ER^{\frac{1}{2}}\delta^{\frac{3}{2}} & \delta<\delta_c\\ \dfrac{4}{3}E\left(R_{ep}^{e}\right)^{\frac{1}{2}}\left(\delta-\delta_r\right)^{\frac{3}{2}} & \delta_c\le\delta<\delta_p\\ \dfrac{4}{3}E\left(R_{p}^{e}\right)^{\frac{1}{2}}\left(\delta-\delta_r\right)^{\frac{3}{2}} & \delta\ge\delta_p\end{cases} \tag{3}$$

where R_{ep}^{e} is the radius of curvature after impact in the elastoplastic phase, $R_{ep}^{e}=\dfrac{P^{e}R}{P_{\max}}$, $P^{e}=\dfrac{4}{3}ER^{\frac{1}{2}}\delta_c^{\frac{3}{2}}$. R_{p}^{e} is the radius of curvature after impact in the plastic phase, $R_{p}^{e}=\dfrac{P_p^{e}R}{P_p}$ $P_p^{e}=\dfrac{4}{3}ER^{\frac{1}{2}}\delta_p^{\frac{3}{2}}$.

The stored energy in the unloading process can be expressed as

$$U_r=\begin{cases}\dfrac{8}{15}ER^{\frac{1}{2}}\delta_{\max}^{\frac{5}{2}} & \delta_{\max}<\delta_c\\ \dfrac{8}{15}E\left(R_{ep}^{e}\right)^{\frac{1}{2}}\left(\delta_{\max}-\delta_r\right)^{\frac{5}{2}} & \delta_c\le\delta_{\max}<\delta_p\\ \dfrac{8}{15}E\left(R_{p}^{e}\right)^{\frac{1}{2}}\left(\delta_{\max}-\delta_r\right)^{\frac{5}{2}} & \delta_{\max}\ge\delta_p\end{cases} \tag{4}$$

3. Hysteresis damping factors

The energy dissipation during the contact process is represented by the hysteresis damping factor that is often a function of the contact stiffness and CoR. The entire contact process undergoes the elastic, elastoplastic, and full plastic phases in sequence. Although the contact stiffness coefficients at the different contact phases can be abstracted from Eq. (1), they make the relationships between the load and displacement exhibits the linear and nonlinear properties at the same time. At the beginning of the contact behavior, the impact behavior is governed by the Hertz contact law; the relationship between the load and deformation is nonlinear[74]. However, the contact stiffness coefficient seems highly nonlinear related to the contact deformation via the Ma-Liu model when the contact comes into the elastoplastic or plastic phase. Actually, the contact stiffness coefficients can be linearized in the elastoplastic or plastic phase [4]. When the contact behavior is equivalently approximated as a single degree of freedom vibration system shown in Fig.3, the effect of the different contact stiffness coefficients on the hysteresis damping factor cannot be ignored. Therefore, this section treats the contact behavior as a nonlinear vibration system in the elastic phase. Nevertheless, once the elastoplastic or plastic deformation is activated, the contact behavior is taken as a linear vibration system. The derivation of the hysteresis damping factors in the different contact phases should be implemented respectively. The initial contact deformation is zero, and the initial impact velocity is assumed as $\dot{\delta}^{(-)}$. The initial conditions are used to determine the amplitude and phase angle of the vibration system [23].

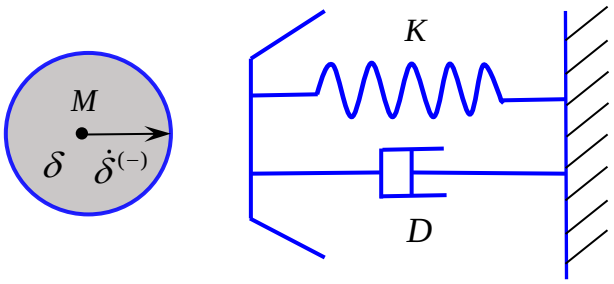

Fig.3 Equivalent vibration system for the contact behavior

3.1. Nonlinear hysteresis damping factor in the elastic phase

At the beginning of the contact, the relation between the force and deformation follows the Hertz contact law. The impact behavior is equivalent to a nonlinear vibration system, which is expressed as

$$M\ddot{\delta} + D_e\dot{\delta} + K_e\delta^{\frac{3}{2}} = 0 \tag{5}$$

where M is the equivalent mass of the system; D_e is a nonlinear hysteresis damping factor. It is worth noting that Eq. (5) has no analytical solution. Hence, the nonlinear hysteresis damping factor only can be approximately solved by the numerical method.
Newton's CoR is assumed as a constant value, which is written as

$$e = -\frac{v_i}{v_0} = -\frac{\dot{\delta}_i}{\dot{\delta}^{(-)}},\ v_i = \dot{\delta}_i,\ v_0 = \dot{\delta}^{(-)} \tag{6}$$

where v_i is the relative impact velocity after impact.

In the elastic phase, the spring force $K_e\delta^{\frac{3}{2}}$ is nonlinear. Moreover, since the damping coefficient D_e is closely related to the nonlinear spring force, the nonlinear damping coefficient is assumed as [75]

$$D_e = \chi_e\delta^{\frac{3}{2}} \tag{7}$$

where χ_e is the nonlinear hysteresis damping factor in the elastic contact phase.

According to this assumption, Eq. (5) can be rewritten as

$$\ddot{\delta} + \frac{\chi_e}{M}\delta^{\frac{3}{2}}\dot{\delta} + \frac{K_e}{M}\delta^{\frac{3}{2}} = 0 \Rightarrow \ddot{\delta} + \beta_1\delta^{\frac{3}{2}}\dot{\delta} + \beta_2\delta^{\frac{3}{2}} = 0, \beta_1 = \frac{\chi_e}{M}, \beta_2 = \frac{K_e}{M} \tag{8}$$

Defining these equations: $v = \dot{\delta}$ and $\dot{v} = \ddot{\delta}$, hence, $dv/d\delta = \dot{v}/\dot{\delta}$. Combining the above equation with Eq. (5), Eq. (7)

$$\frac{dv}{d\delta} = \frac{-\beta_1\delta^{\frac{3}{2}}\dot{\delta} - \beta_2\delta^{\frac{3}{2}}}{v} \Rightarrow vdv = -\left(\beta_1 v + \beta_2\right)\delta^{\frac{3}{2}}d\delta \tag{9}$$

Eq. (9) can be integrated over the impact process, which is written as

$$\int_{v_0}^{v}\frac{v}{\beta_1 v + \beta_2}dv = -\int_{\delta_0}^{\delta_i}\delta^{\frac{3}{2}}d\delta \Rightarrow \left(\beta_1 v - \beta_2\ln\left(\beta_1 v + \beta_2\right)\right)\Big|_{v_0}^{v} = -\frac{5}{2}\beta_1^2\delta^{\frac{5}{2}}\Big|_{\delta_0}^{\delta_i} \tag{10}$$

Using the initial conditions $\delta_0 = \delta_i = 0, v = -ev_0$, Eq. (10) is rewritten as using Taylor expansion

$$\begin{aligned}
&\beta_1 v-\beta_2\left[\ln\beta_2+\ln\left(1+\frac{\beta_1}{\beta_2}v\right)\right]=-\frac{5}{2}\beta_1^2\delta_i^{\frac{5}{2}}+\beta_1 v_0-\beta_2\left[\ln\beta_2+\ln\left(1+\frac{\beta_1}{\beta_2}v_0\right)\right]\\
&\Rightarrow \beta_1 v-\beta_2\ln\left(1+\frac{\beta_1}{\beta_2}v\right)=\beta_1 v_0-\beta_2\ln\left(1+\frac{\beta_1}{\beta_2}v_0\right)\\
&\Rightarrow \beta_1 v-\beta_2\left(\beta v-\frac{1}{2}\beta^2v^2+\frac{1}{3}\beta^3v^3+\ldots\right)=\beta_1 v_i-\beta_2\left(\beta v_0-\frac{1}{2}\beta^2v_0^2+\frac{1}{3}\beta^3v_0^3+\ldots\right)
\end{aligned}\tag{11}$$

where $\beta=\beta_1/\beta_2=\chi_e/K_e$.

The dissipated energy during contact is closely related to the CoR [9,17], the assumption that the CoR is linear with the initial impact velocity is implemented. The CoR can be approximately expressed as

$$e=1-\alpha\dot{\delta}^{(-)}=1-\alpha v_0 \tag{12}$$

where α is the coefficient of the polynomial.
Substituting Eq. (12) into Eq. (11)

$$\begin{aligned}
&\frac{1}{2}\beta_2\beta^2v^2-\frac{1}{3}\beta_2\beta^3v^3=\frac{1}{2}\beta_2\beta^2v_0^2-\frac{1}{3}\beta_2\beta^3v_0^3\\
&\Rightarrow\frac{1}{2}\beta^2\left[\left(1-\alpha v_0\right)v_0\right]^2+\frac{1}{3}\beta^3\left[\left(1-\alpha v_0\right)v_0\right]^3=\frac{1}{2}\beta^2v_0^2-\frac{1}{3}\beta^3v_0^3\\
&\Rightarrow\frac{1}{2}\beta^2v_0^2-\alpha\beta^2v_0^3+\frac{1}{2}\alpha^2\beta^2v_0^4+\frac{1}{3}\beta^3v_0^3\left(1-3\alpha v_0+3\alpha^2v_0^2-\alpha^3v_0^3\right)=\frac{1}{2}\beta^2v_0^2-\frac{1}{3}\beta^3v_0^3\\
&\Rightarrow-\alpha\beta^2v_0^3+\frac{1}{2}\alpha^2\beta^2v_0^4+\frac{2}{3}\beta^3v_0^3-\alpha\beta^3v_0^4+\alpha^2\beta^3v_0^5-\frac{1}{3}\alpha^3\beta^3v_0^6=0\\
&\Rightarrow-\alpha+\frac{1}{2}\alpha^2v_0+\frac{2}{3}\beta-\alpha\beta v_0+\alpha^2\beta v_0^2-\frac{1}{3}\alpha^3\beta v_0^3=0
\end{aligned}\tag{13}$$

Since the coefficient of the polynomial can be expressed as $\alpha=\left(1-e\right)/v_0$ based on Eq. (12), one has the alternative formulation after ignoring the high order α^3

$$\begin{aligned}
&\frac{2}{3}\beta-\alpha\beta v_0+\alpha^2\beta v_0^2-\frac{1}{3}\alpha^3\beta v_0^3=\alpha-\frac{1}{2}\alpha^2v_0\Rightarrow\beta\left(\frac{2}{3}-\alpha v_0+\alpha^2v_0^2\right)=\alpha-\frac{1}{2}\alpha^2v_0\\
&\Rightarrow\beta\left(\frac{2}{3}-\left(1-e\right)+\left(1-e\right)^2\right)=\frac{1-e}{v_0}-\frac{\left(1-e\right)^2}{2v_0}\Rightarrow\beta=\frac{3\left(1-e^2\right)}{2\left(2-3e+3e^2\right)v_0}
\end{aligned}\tag{14}$$

Therefore, the nonlinear hysteresis damping factor represents the energy dissipation caused by the seismic waves [32] can be expressed as

$$\chi_e=\frac{3K_e\left(1-e^2\right)}{2\left(2-3e+3e^2\right)v_0} \tag{15}$$

Finally, the novel dashpot model in the elastic phase can be obtained according to the nonlinear vibration system

$$F=K_e\delta^{\frac{3}{2}}+D_e\dot{\delta}=K_e\delta^{\frac{3}{2}}\left[1+\frac{3\left(1-e^2\right)}{2\left(2-3e+3e^2\right)}\frac{\dot{\delta}}{\dot{\delta}^{(-)}}\right] \tag{16}$$

3.2. Linear hysteresis damping factor in the elastoplastic or plastic phase

When the contact comes into the elastoplastic or plastic phase, since the relationship between the contact force and deformation approximates the linear based on the Ma-Liu model [4], the equivalent contact stiffnesses coefficient is expressed as

$$K = \left(P_{ep} - P_c\right) / \left(\delta_p - \delta_c\right) \tag{17}$$

Therefore, the impact behavior is treated as a linear vibration system. Its equation of motion can be written as

$$M\ddot{\delta} + D\dot{\delta} + K\delta = 0 \tag{18}$$

where D is the linear damping function.

The linear damping coefficient is assumed as the linear function of the contact deformation, which is expressed as [23,26]

$$D = C\delta \tag{19}$$

where C is the linear damping factor. This assumption can guarantee the positive value of the contact force and continuous relationship between the contact force and deformation no matter what in the elastic or elastoplastic contact phase [26][15,76,77].

According to Eq. (19), Eq. (18) can be rewritten as

$$M\ddot{\delta} + \left(C\dot{\delta} + K\right)\delta = 0 \tag{20}$$

The solution of Eq. (18) is expressed as

$$\delta(t) = A\sin\left(\omega t + \phi\right) \tag{21}$$

where A is the amplitude of vibration, ϕ is the phase angle, t is the duration of contact, the frequency of vibration is written as

$$\omega = \sqrt{\frac{C\dot{\delta} + K}{M}} \tag{22}$$

Based on the initial condition, the following equations can be obtained

$$\begin{cases} t = 0, \delta = 0 \Rightarrow 0 = \sin\left(\phi\right) \\ t = 0, \dot{\delta} = \dot{\delta}^{(-)} \Rightarrow \dot{\delta}^{(-)} = A\omega\cos\left(\phi\right) \end{cases} \Rightarrow \phi = 0, A = \frac{\dot{\delta}^{(-)}}{\omega} \tag{23}$$

Therefore, Eq. (21) is rewritten as

$$\delta(t) = \frac{\dot{\delta}^{(-)}}{\omega}\sin\left(\omega t\right) \tag{24}$$

The Eq. (24) can be approximated using Taylor expansion

$$\delta(t) = \frac{\dot{\delta}^{(-)}}{\omega}\left[\omega t - \frac{1}{3!}\left(\omega t\right)^3 + \frac{1}{5!}\left(\omega t\right)^5 + \ldots\right] \tag{25}$$

Substitute Eq. (22) into Eq. (25)

$$\begin{aligned}\delta(t) &= \dot{\delta}^{(-)}\left[t-\frac{1}{6}\omega^2 t^3+\frac{1}{120}\omega^4 t^5+\ldots\right] \\ &= \dot{\delta}^{(-)}t-\frac{C\dot{\delta}^{(-)}+K}{6M}\dot{\delta}^{(-)}t^3+\frac{\left(C\dot{\delta}^{(-)}+K\right)^2}{120M^2}\dot{\delta}^{(-)}t^5+\ldots\end{aligned} \tag{26}$$

The relative contact velocity after impact can be written as

$$\begin{aligned}\dot{\delta}(t) &= \dot{\delta}^{(-)}\left[1-\frac{1}{2}\omega^2 t^2+\frac{1}{24}\omega^4 t^4+\ldots\right] \\ &= \dot{\delta}^{(-)}-\frac{C\dot{\delta}^{(-)}+K}{2M}\dot{\delta}^{(-)}t^2+\frac{\left(C\dot{\delta}^{(-)}+K\right)^2}{24M^2}\dot{\delta}^{(-)}t^4+\ldots\end{aligned} \tag{27}$$

where t corresponds to the time when two contact bodies are separating. It is expressed as

$$t=\frac{\pi}{2\omega_r},\omega_r=\sqrt{\frac{K}{M}} \tag{28}$$

According to Eq. (27), Newton's CoR in Eq. (6) is rewritten as

$$\begin{aligned}e &= 1-\frac{C\dot{\delta}^{(-)}+K}{2M}t^2+\frac{\left(C\dot{\delta}^{(-)}+K\right)^2}{24M^2}t^4+\ldots \\ &= 1-\frac{Kt^2}{2M}-\frac{Ct^2}{2M}\dot{\delta}^{(-)}+\frac{C^2\left[\dot{\delta}^{(-)}\right]^2+2KC\dot{\delta}^{(-)}+K^2}{24M^2}t^4 \\ &= 1-\frac{Kt^2}{2M}+\frac{K^2t^4}{24M^2}-\left(1-\frac{Kt^2}{6M}\right)\frac{Ct^2}{2M}\dot{\delta}^{(-)}+\frac{C^2t^4}{24M^2}\left[\dot{\delta}^{(-)}\right]^2+\ldots\end{aligned} \tag{29}$$

Compared Eq. (12) with Eq. (29), the equation in allusion to $\dot{\delta}^{(-)}$ can be established as

$$\left(1-\frac{Kt^2}{6M}\right)\frac{Ct^2}{2M}=\alpha \tag{30}$$

Hence, the linear damping factor is solved as

$$C=\frac{2M\alpha}{\left(1-\frac{Kt^2}{6M}\right)t^2} \tag{31}$$

Substitute Eq. (28) into Eq. (31), the damping factor is expressed as

$$C=\frac{2M\alpha}{\left(1-\frac{Kt^2}{6M}\right)t^2}=\frac{2M\alpha}{\left(1-\frac{K}{6M}\cdot\frac{\pi^2M}{4K}\right)\frac{\pi^2M}{4K}}=\frac{8K\alpha}{\pi^2\left(1-\frac{\pi^2}{24}\right)}=\frac{192K\alpha}{\pi^2\left(24-\pi^2\right)} \tag{32}$$

The linear damping factor is expressed as based on Eq. (19)

$$D=\frac{192K\alpha\delta}{\pi^2\left(24-\pi^2\right)} \tag{33}$$

Substitute Eq. (12) into Eq. (33), the damping factor is rewritten as

$$D=\frac{192(1-e)K}{\pi^2\left(24-\pi^2\right)}\frac{\delta}{\dot{\delta}^{(-)}} \tag{34}$$

Combining Eq. (18) with Eq. (34), the novel contact force model with the elastoplastic deformation and hysteresis damping factor can be written as

$$F = K\delta\left[1+\frac{192\left(1-e\right)}{\pi^2\left(24-\pi^2\right)}\frac{\dot{\delta}}{\dot{\delta}^{(-)}}\right] \tag{35}$$

Combing Eq. (16) with Eq. (35), a comprehensive dashpot model including the elastic, elastoplastic, and plastic phases can be formulated as

$$F=\begin{cases} K_e\delta^{\frac{3}{2}}\left[1+\dfrac{3\left(1-e^2\right)}{2\left(2-3e+3e^2\right)}\dfrac{\dot{\delta}}{\dot{\delta}^{(-)}}\right] & \left(\delta\le\delta_c\right) \\ K\delta\left[1+\dfrac{192\left(1-e\right)}{\pi^2\left(24-\pi^2\right)}\dfrac{\dot{\delta}}{\dot{\delta}^{(-)}}\right] & \left(\delta>\delta_c\right) \end{cases} \tag{36}$$

4. CoR for the different contact phases

The CoR plays an essential role in evaluating the dissipated energy during contact [8,9,11,29,71]. The contact behavior is divided into elastic, elastoplastic, and plastic phases. In each contact deformation phase, the kinetic energy would be dissipated more or less. In the elastic deformation phase, the contact body seismic waves produce an energy loss in the impact region. The seismic waves include compression waves, shear waves, and Rayleigh waves. Most of the seismic waves' energy travels as surface waves with around 67% of the Rayleigh waves' radiated energy, 7% in the compression waves, and 26% in the shear waves [32]. The CoR in the elastic contact phase is expressed as

$$\mathrm{CoR}_e = \exp\left(-0.6\frac{c_0}{c_2}\left(\frac{\dot{\delta}^{(-)}}{c_0}\right)^{3/5}\right) \tag{37}$$

where c_0 is the compressional wave velocity written as $c_0=\sqrt{E/\rho}$. c_2 is the shear wave velocity written as $c_2=\sqrt{G/\rho}$, $G=E/\left(2\left(1+\nu\right)\right)$. ρ is density.

When the initial impact velocity activates the plastic deformation, the CoR is identified by the Ma-Liu model, which can be written as

$$\mathrm{CoR}=\sqrt{\frac{U_r}{U_c}} \tag{38}$$

where U_r is the stored energy after impact in the restitution phase, U_c is the work done by the contact force in the compressional phase.

5. Dynamic performance analysis of the new dashpot model

A spherical clearance joint is taken as an example in this section. The simulation parameters are assumed as in Table 1. The ratio ψ is equal to 3.0, the dimensionless parameter ε corresponding to a geometric relationship is assumed as 13.

Table 1. Contact parameters

Element	Young's modulus (Pa)	Poisson ratio	Radius (m)	Yield strength (Pa)	Density (kg/m^3)
Body 1	2.0×10^{11}	0.29	2.00×10^{-2}	1.03×10^{9}	7800
Body 2	6.5×10^{10}	0.33	2.05×10^{-2}	3.00×10^{7}	2700

5.1. Dynamic behavior in the elastic phase

As for the new dashpot model, Hertz contact stiffness is equal to 6.6E10 N/m$^{1.5}$. The elastoplastic deformation is not activated when the initial impact velocity equals 0.02 m/s. The CoR in Eq. (37) is evaluated as 0.9995, which illuminates that the energy dissipation caused by the seismic waves is negligible. Although the hysteresis loop produced by the nonlinear hysteresis damping factor almost disappears in Fig.4, the new dashpot model still can describe the energy dissipation in the elastic contact phase. On the contrary, the Ma-Liu model considered that the contact behavior in the elastic phase follows Hertz contact law in the loading and unloading path, which neglects the dissipated energy caused by seismic waves.

Moreover, in order to exhibit the merit of the new dashpot model in the elastic phase, the CoR is assumed as 0.8, at the same time, three representative dashpot models extended based on the Hertz contact law, including the Hunt-Crossley, Lankarani-Nikravesh, and Flores et al. models are treated as the benchmark solution to evaluate the accuracy of the new dashpot model in the elastic phase. According to the definition of Newton's CoR, the post-impact velocity should be $\dot{\delta} = -e\dot{\delta}^{(-)}$ that is equal to -0.016 m/s. Comparison analysis between the new dashpot model and existing dashpot models is implemented; the post-impact velocities from the different dashpot models can be seen in Fig. 5. Although these contact velocities are close to each other, their discrepancy displays the high-accuracy dashpot model. The impact velocities from the Hunt-Crossley, Lankarani-Nikravesh, and Flores et al., and new dashpot models equal -0.0167 m/s, -0.0169 m/s, -0.0157 m/s, and -0.0162 m/s, respectively. Significantly, the post-impact velocity from the new dashpot model is more closed to -0.016 m/s compared to the other dashpot models, which illuminates that the new dashpot model possesses high accuracy in the elastic phase.

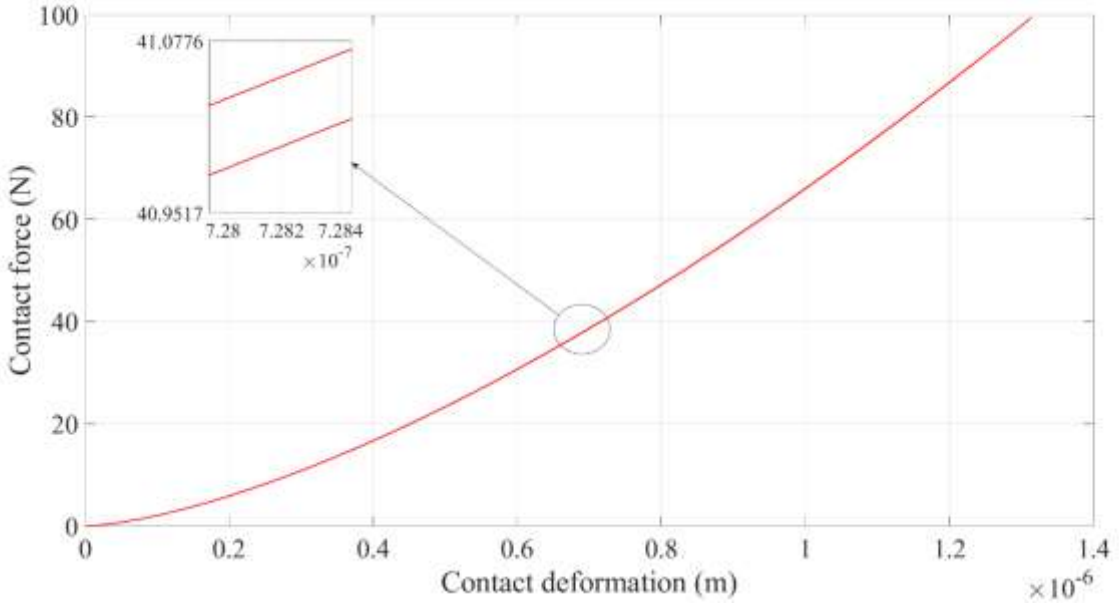

Fig.4 Dynamic performance of the elastic phase

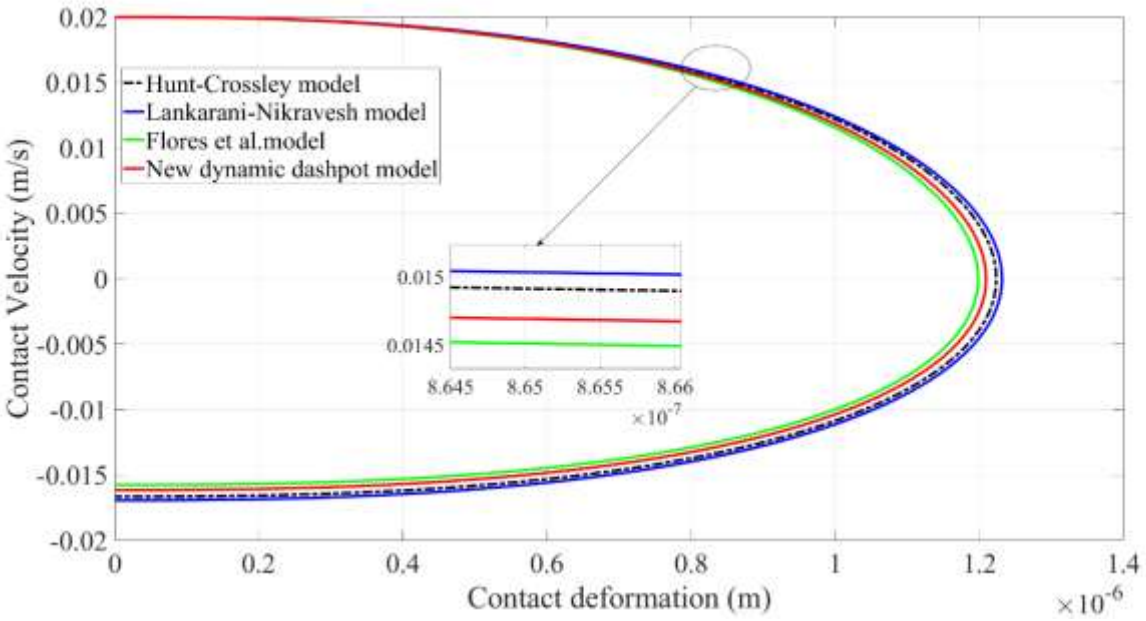

Fig.5 The accuracy analysis between the new dashpot model and existing dashpot models

5.2. Dynamic responses in the elastoplastic phase

When the initial impact velocity has a moderate value equal to 4 m/s, the contact deformation surpasses the critical elastic deformation that is 1.5788E-6 m. The maximum contact deformation calculated using the Ma-Liu model equals 1.1152E-4 m. The dynamic responses of this system obtained by the Ma-Liu model can be seen in Fig. 6. Hence, the CoR can be identified as 0.6909 by Eq. (38) when the elastoplastic deformation is activated. In Fig.6, when the contact behavior is in the elastic contact phase, the loading path is the same as the unloading path. There is no energy dissipated. When the contact deformation exceeds the critical elastic deformation, the loading path is different from the unloading path. The area consists of the loading and unloading paths, which represents the dissipated energy during contact.

The dynamic response of this system can be evaluated by the new dashpot model once the CoR is obtained by the Ma-Liu model, which is displayed in Fig.7. The energy dissipation caused by the seismic waves is considered using the new nonlinear damping factor in the new dashpot model. Likewise, when the contact deformation surpasses the critical elastic deformation, the energy dissipation caused by the elastoplastic deformation is measured by the new linear damping factor as well in Fig.7. As for the new dashpot model, since its first term is the same as the Ma-Liu model, the maximum contact deformation in Fig.6 obtained by the Ma-Liu model cannot be reached using the new dashpot model in the presence of the damping terms. The mathematical form of two kinds of contact models determines this deviation. However, the contact responses calculated by the new dashpot model can keep harmonious with the Ma-Liu model overall no matter what regarding the contact force or energy dissipation during contact. Therefore, the new dashpot model provides a concise form for simulating the elastoplastic contact behavior, which does not need to distinguish the compression and recovery phase in the calculation process. Furthermore, the maximum contact deformation and the residual deformation must be saved in every collision when the contact behavior is evaluated by the Ma-Liu model, which is not beneficial for the programming, especially in the multi-contact and multi-compression behavior during impact.

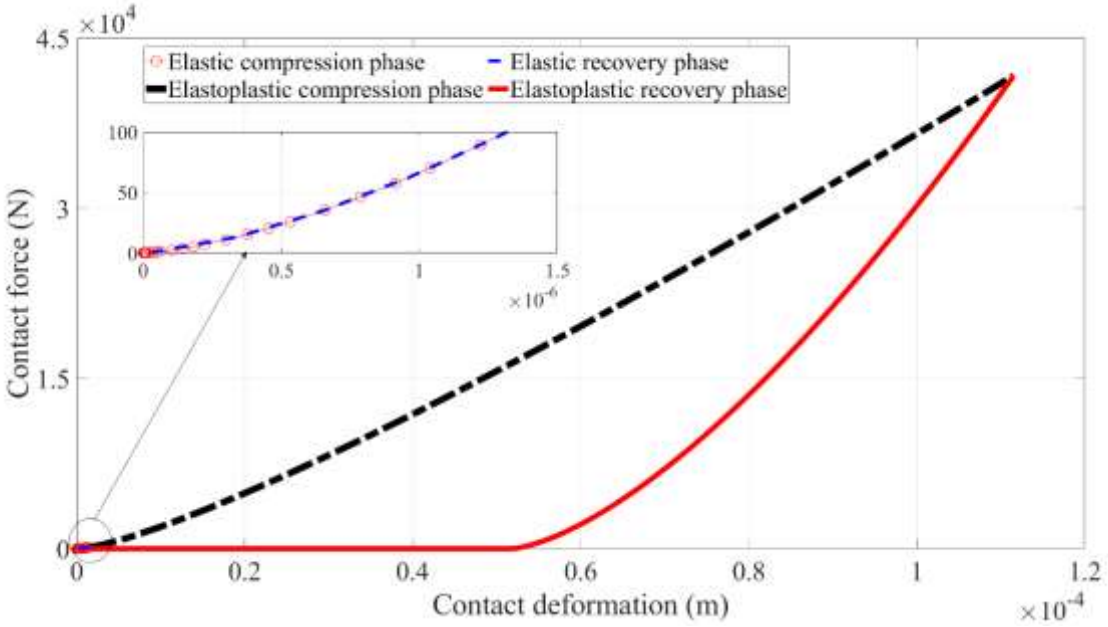

Fig.6 Dynamic performance obtained by the Ma-Liu model when the elastoplastic deformation is activated

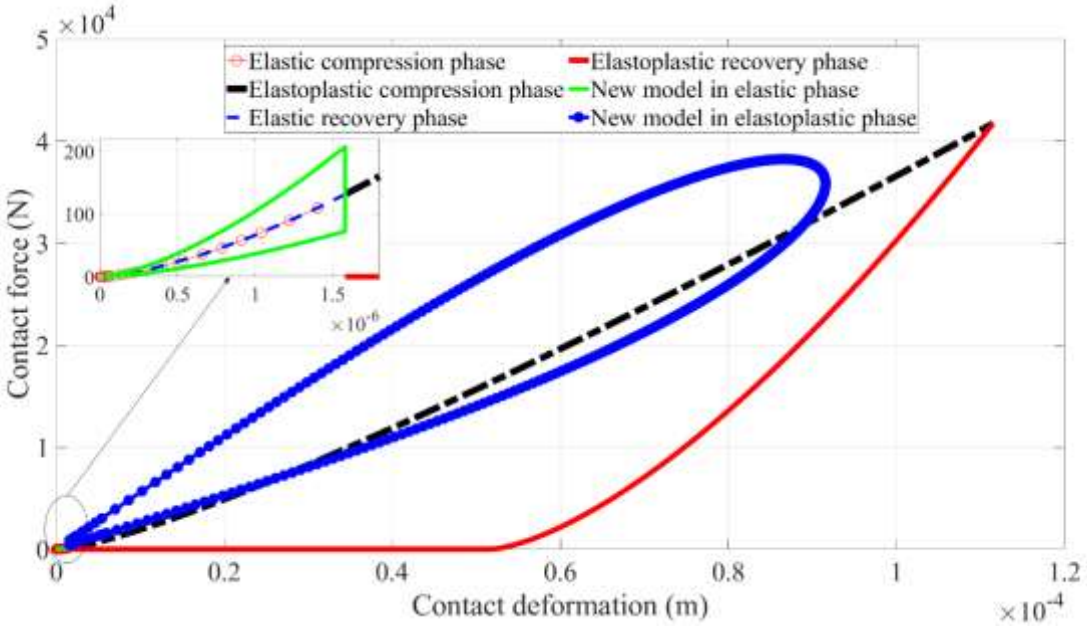

Fig.7 Comparison between the new dashpot model and Ma-Liu model in the elastoplastic phase

5.3. Dynamic responses in the plastic phase

When the initial impact velocity is equal to 6 m/s, the contact deformation exceeds the critical plastic deformation 1.3340E-4 m. The maximum contact deformation calculated using the Ma-Liu model equals 1.6082E-4 m. The dynamic responses of this system obtained by the Ma-Liu model can be seen in Fig. 8. The CoR can be identified as 0.6558 based on Eq. (38) when the plastic deformation is activated. The entire contact behavior includes the elastic, elastoplastic, and plastic phases simultaneously. When the contact deformation exceeds the critical plastic deformation, the plastic phase is governed by Eq. (1) in the compression phase and Eq. (3) in the recovery phase. Within the elastoplastic phase, the dynamic performances in Fig. 8 are consistent with Fig. 6. When the CoR in the new dashpot model is identified using the Ma-Liu model.

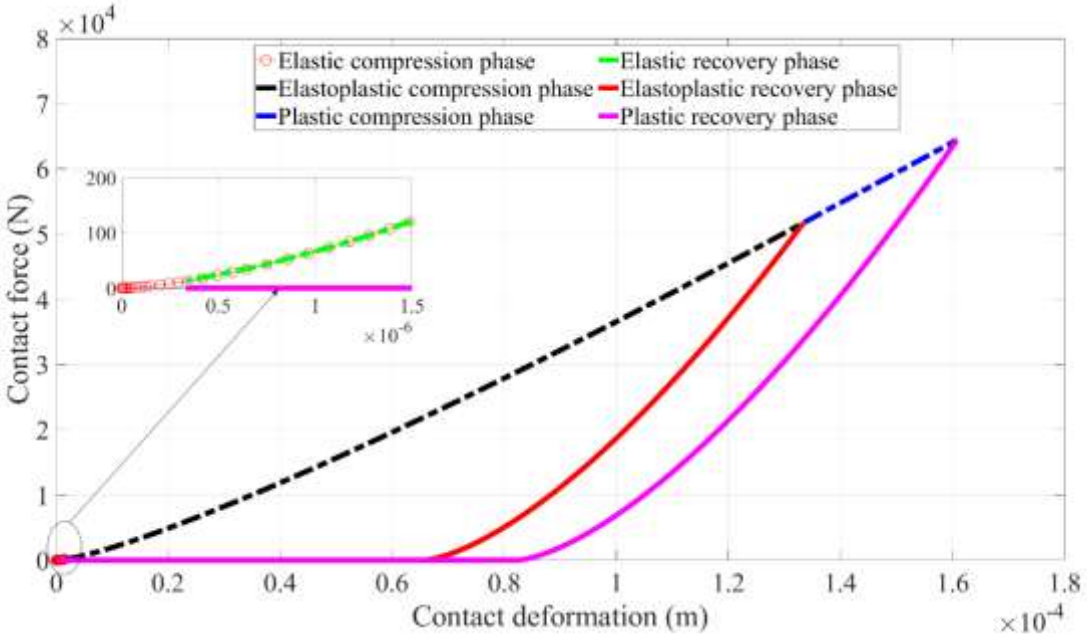

Fig.8 Dynamic responses obtained by the Ma-Liu model when the plastic deformation is activated

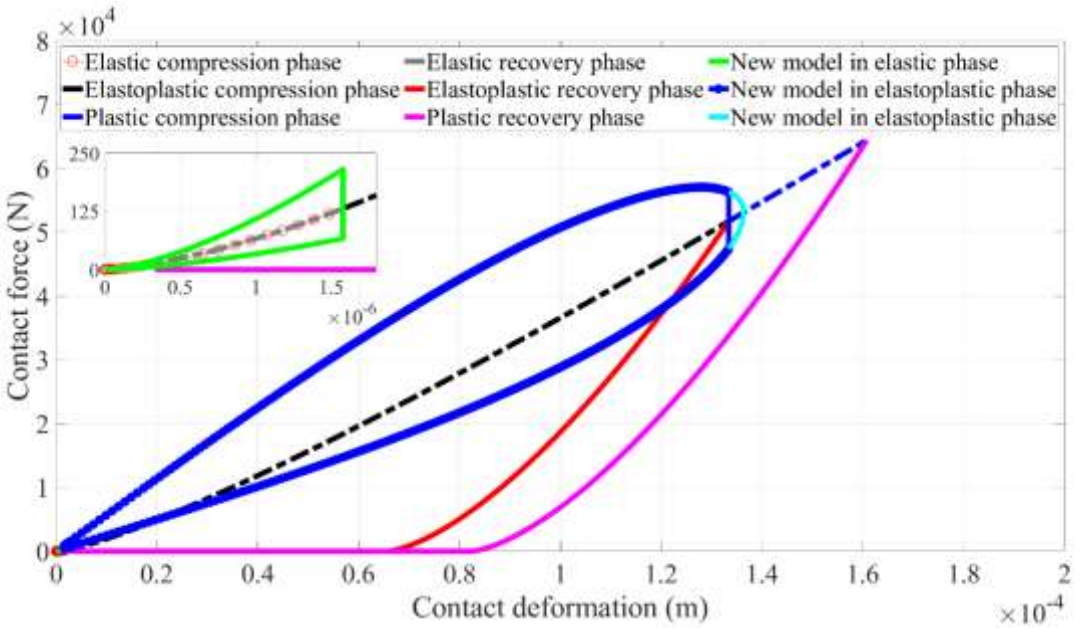

Fig.9 Comparison between the new dashpot model and Ma-Liu model in the plastic phase

The hysteresis loop in Fig.9 represents energy dissipation caused by the elastoplastic deformation and includes the energy dissipation caused by the seismic waves in the elastic phase. This new dashpot model makes up for the deficiency ignoring the energy dissipation caused by the seismic waves in the elastic phase of the Ma-Liu model. In a word, the new dashpot model can describe the energy dissipation corresponding to each contact phase by the nonlinear and linear hysteresis damping factors and keep harmonious with the Ma-Liu model overall.

5.4. Comparison between the contact models

Although the existing dashpot models developed based on the Hertz law are suited for calculating the elastic impact behavior with low impact velocity, they in somewhere are used to estimate the impact behavior with elastoplastic deformation under relatively high impact velocity by regulating the CoR.

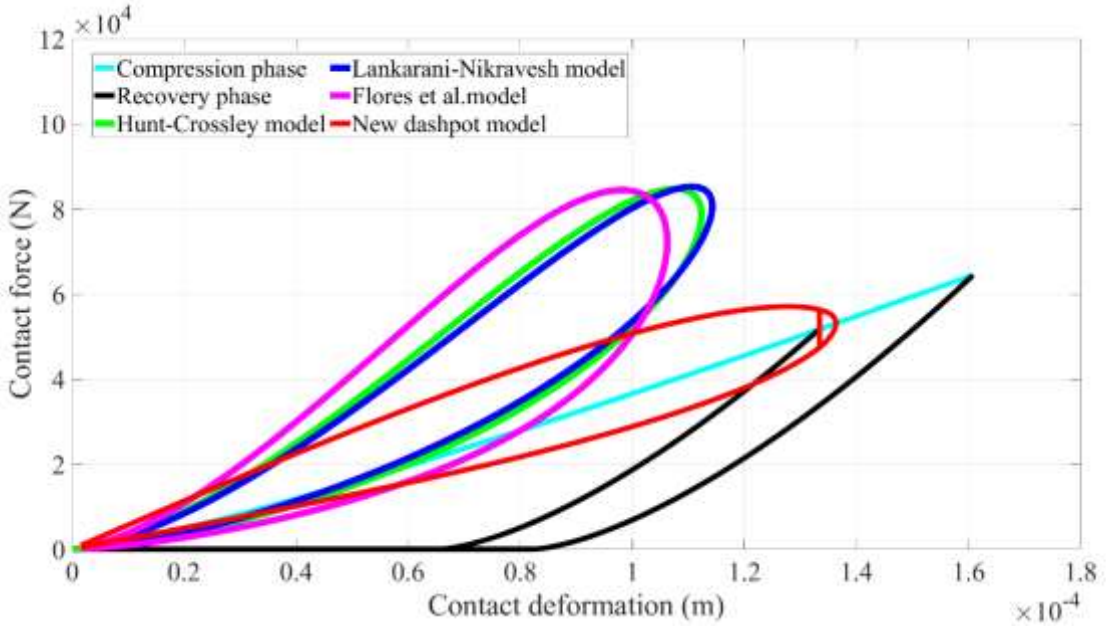

Fig.10 Comparison between the new dashpot model and existing dashpot models

This section treats the Ma-Liu model as the reference solution to judge which dashpot model is suited for the elastoplastic impact scenario in Fig. 10. In section 5.1, the Hertz contact stiffness equals 6.6E10 $N/m^{1.5}$; however, when the elastoplastic deformation is activated, the linearized contact stiffness equals 3.8765E8 N/m. Conspicuously, the Hertz contact stiffness overestimates the contact stiffness in the elastoplastic phase [68]. That is why the maximum contact forces from the Hunt-Crossley, Lankarani-Nikravesh, and Flores et al. models are significantly larger than the one obtained from the Ma-Liu model. On the contrary, when the Hertz contact stiffness is replaced by the linearized elastoplastic contact stiffness from the Ma-Liu model, the maximum contact force obtained from the new dashpot model keeps harmonious with the Ma-Liu model in Fig. 10. This conclusion illustrates that the existing dashpot models will produce a significant error when calculating the elastoplastic impact behavior with relatively high impact velocity. In sharp contrast, the new dashpot model can accurately evaluate the maximum contact force and simplify the calculation process of the Ma-Liu model in allusion to the elastoplastic contact behavior.

6. The new dashpot model applied in multibody system

In the mechanical system, the clearance in the joint is an inevitable phenomenon because of the manufacturing error and wear behavior[78]. The high-frequency contact force arises from the clearance joint, which makes the mechanical system produce significant tremble and instability[79]. This situation threatens the safe operation of the mechanical system seriously[80,81]. It is necessary to study the effect of the clearance joint on the dynamic performance of the multibody system[82]. Although this topic experiences around twenty years of development, it seldom considers the elastoplastic deformation between the joint clearance elements[79]. Therefore, the trajectory and velocity of the multibody system with clearance joint are not sensitive to the contact between the clearance joint elements because the contact deformation is limited within the elastic deformation [66]. However, when the impact between the clearance joint elements activates the elastoplastic deformation[83], the dynamic responses of the multibody system have a significant difference from the previous dynamic performances considering the elastic deformation only during contact. In order to identify the effect of the elastic and plastic deformation in the clearance joint on the dynamic

responses of the multibody system, the slider-crank mechanism with clearance joint in Fig. 11 is taken as a numerical example. The revolute joint between link 3 and the slider is treated as a clearance joint. The slider-crank mechanism's structure parameters [82] are displayed in Table 2. The contact parameters [82] can be seen in Table 3. The drive velocity of the crank is 200 rpm.

Table 2. Structure parameters of the slider-crank mechanism

Components	Mass (kg)	Length (m)	Moment of inertia (kg.m^2)
Crank	17.900	0.05	0.460327
Connecting rod	1.130	0.30	0.015300
Sliding block	1.013	-	0.000772

Table 3. Simulation parameters

Parameters	Value
Young's modulus	207 GPa
Poisson's ratio	0.3
Radius of journal	0.0095 m
Radius of bearing	0.01 m
Coefficient of restitution	0.46
Dynamic friction coefficient	0.01
Initial contact velocity	0.5 m/s
Integrator	Ode45
Timestep	1E-4 s

The normal contact force is calculated using the new dashpot model, the tangential contact force is estimated based on the modified Coulomb friction model[84]. In this friction model, a dynamic coefficient can avoid the discontinuity phenomenon, which is in order to achieve a continuous friction force-velocity relationship. The modified Coulomb friction model can be written as [85]

$$\mathbf{F}_t = -\mu(v_t) F_n \frac{\mathbf{v}_t}{|\mathbf{v}_t|} \tag{39}$$

where F_n is the normal contact force; $\mathbf{v}_t$ is the tangential velocity vector. $\mu(v_t)$ is the dynamic friction coefficient, which can refer to this literature [55].

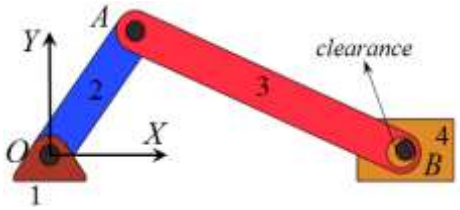

Fig.11 Slider-crank mechanism with clearance revolute joint

6.1. Within the scope of the elastic phase

The large yield strength of contact bodies in the clearance revolute joint leads to contact deformation that is hard to exceed the critical elastic deformation equals 9.9735E-5 m. Therefore, the Hertz contact law governs the entire contact behavior. The contact force model in Eq.(16) is selected to simulate the contact behavior happening in the clearance revolute joint.

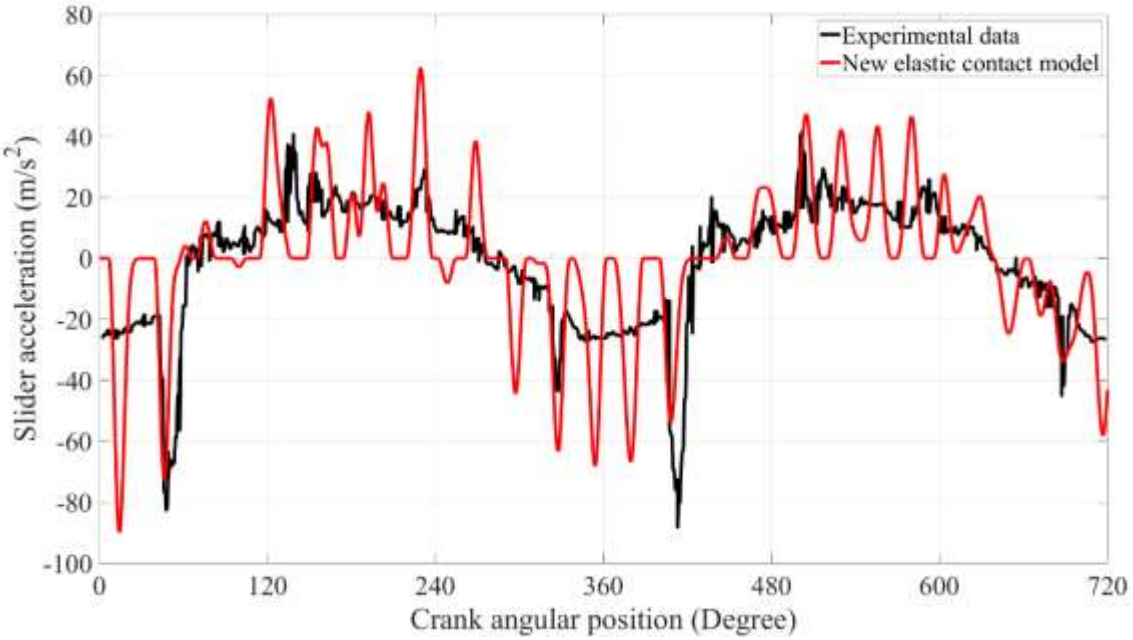

Fig.12 Comparison analysis between the experimental data and new dashpot model

In Fig. 12, the slider's acceleration obtained using the new dashpot model keeps consistent with the experimental data in Fig.11(e) of the reference [82], which illuminates the reasonability of the new dashpot model. Moreover, the traditional dashpot models [5] can also predict the dynamic responses of the slider-crank mechanism with clearance joint. In Fig. 13, the new dashpot model can obtain almost the same solutions as the Lankarani-Nikravesh and Flores et al. models. This conclusion proves that the new dashpot model can successfully depict the contact behavior in the multibody system with the clearance joint. Since the clearance size is very small compared to the link size in the slider-crank mechanism [86,87], the slider displacement is not sensitive to the contact behavior in Fig. 13 (a). On the contrary, the slider acceleration in Fig.13 (b) is conspicuously affected by the contact happening in the clearance joint. The slider acceleration often backs to zero in one period when the journal does not come into contact with the bearing.

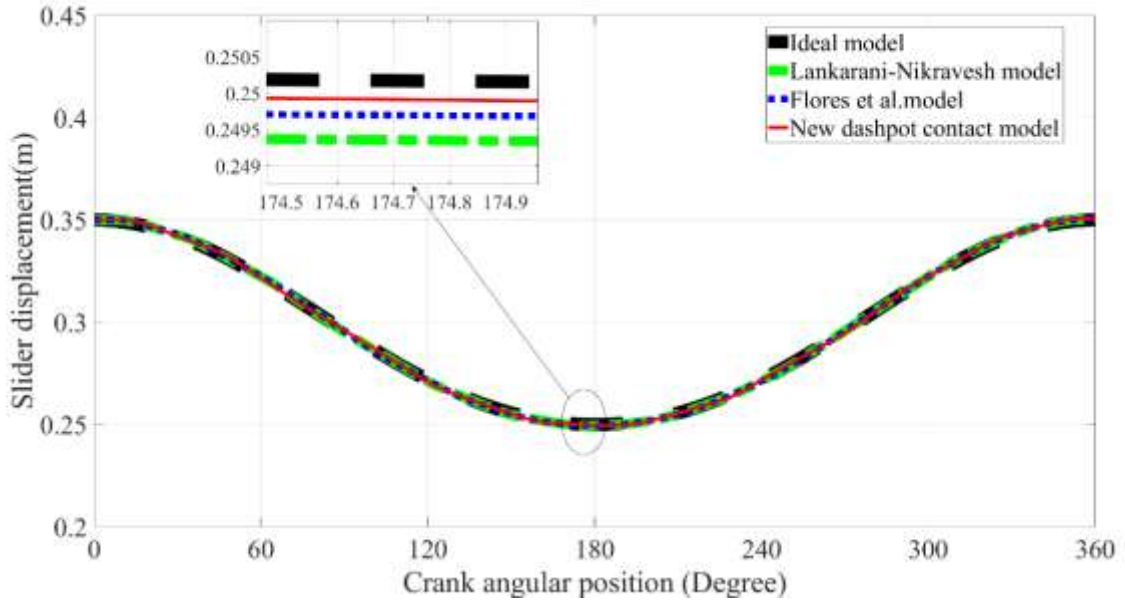

(a)

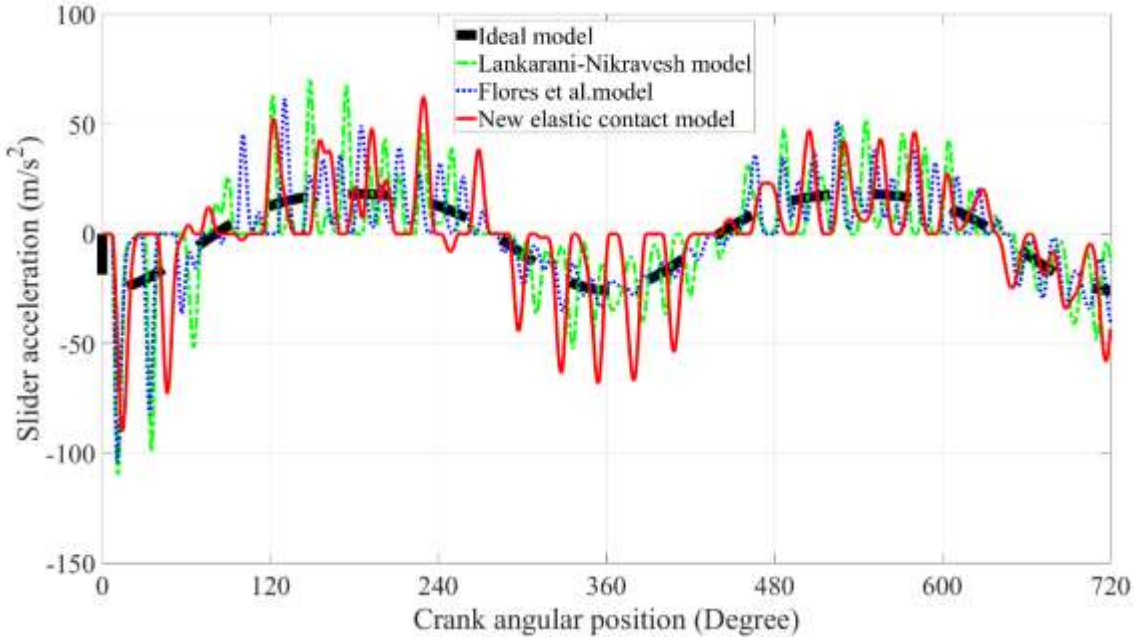

(b)

(a) displacement; (b) acceleration

Fig.13 Dynamics performance of the slider-crank mechanism when only elastic deformation happens

6.2. When the elastoplastic deformation happens in the clearance joint

In Section 6.1, the contact material has a large yield strength, and the entire contact behavior happens within the scope of the elastic deformation. Therefore, the slider displacement and velocity are not sensitive to the contact behavior. In order to illustrate the effect of the elastoplastic deformation on the dynamic performance of the multibody system, the material properties of the revolute joint with clearance are replaced by the other material with small yield strength shown in Table 1.

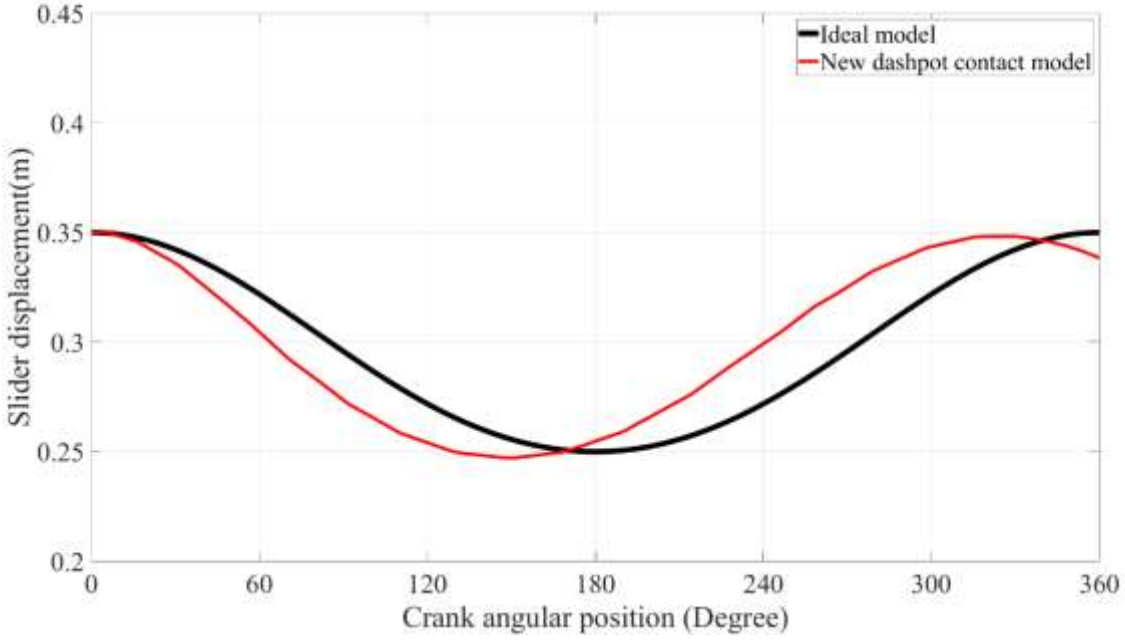

Fig.14 Slider displacement considering the plastic deformation

In this case, the contact behavior in the clearance joint is prone to produce elastoplastic deformation. The crank drive velocity is taken as 300 rpm, the initial impact velocity is assumed as 1.25 m/s. The CoR is identified as 0.8103 using the Ma-Liu model. The maximum contact deformation equals 3.8310E-5 m, which surpasses the critical elastic deformation that is 1.5801E-6 m. Namely, the elastoplastic deformation happens in the revolute joint with clearance of the slider-crank mechanism. The simulations show that the dynamic performance of the slider-crank mechanism with clearance joint is significantly affected by the elastoplastic deformation in Fig. 14. Two primary reasons result in this phenomenon: (i) the contact radius of the bearing becomes significant when the elastoplastic deformation happens, which increases the clearance size further. This situation leads to the slider displacement being conspicuously different from the i deal case in Fig. 14, which is also the reason that makes the displacement delay when considering the elastoplastic deformation during contact. (ii) although the contact stiffness is smaller than the Hertz contact stiffness when the contact status comes into the elastoplastic phase, the power exponent of the contact deformation is equal to 1 rather than 1.5. Furthermore, the elastoplastic deformation results in the slider displacement deviating from the ideal case. When the contact comes into the elastoplastic phase, the contact stiffness in Eq. (17) is the elastoplastic contact stiffness of the Ma-Liu model rather than Hertz contact stiffness. Moreover, the elastoplastic contact stiffness is smaller than the Hertz contact stiffness, which leads to the entire contact process needing more time to be finished in the elastoplastic phase. That is the other reason that results in the delay of the displacement. The conclusions above illuminate adequately that the elastoplastic deformation must be considered in the multibody system when the contact deformation in the contact behavior surpasses the critical elastic deformation.

The significance of this numerical example is in order to exhibit the merits of the proposed contact force model: (i) in section 6.1, the proposed contact model in the elastic phase can obtain a reasonable solution that keeps consistent with the existing contact force models. In addition to this, when the only elastic deformation happens between the joint clearance elements, the slider displacement is not sensitive to the contact behavior and clearance size because the elastic deformation can be ignored compared to the structure size of the slider-crank mechanism. (ii) In contrast to the elastic impact behavior, the slider-crank mechanism is operated at high-speed, and the elastoplastic deformation is activated under impact between the journal and bearing. Obviously, the existing contact models still obtain the conclusion that contact deformation has no effect on the slider displacement because they cannot describe the elastoplastic deformation. That is why we develop the new contact force model, including the elastic, elastoplastic, and plastic phases. In Fig. 14, the elastoplastic deformation makes the curvature of the contact bodies have a significant variation, which leads to the contact behavior between the journal and bearing altering the trajectory of the slider. The sharp contrast analysis between two different numerical examples shows the necessity and rationality of the developmental new contact force model.

6.3. Hopkinson incident bar

In order to validate the effectiveness of the proposed dashpot model in the elastoplastic or plastic phase, Fig.15 is a schematic of the experimental setup of the Hopkinson pressure bar [88]that was used to impact granular chain consisting of 50 identical stainless-steel spheres with diameter 6.35mm. The strain gauges on the incident and transmission bars can be used to measure the incident, reflected, and transmitted stress waves. The spheres were held between the bars and limited to moving along the axis of the plastic tube. A truncated sphere was used as the first particle in flat contact with the end of the incident bar, which guarantees that the first particle had the same velocity as the end of the incident

bar measured by the strain gauges. A copper pulse shaper was applied between the striker and incident bar to produce the repeatable impacts for all experiments [88]. The laser vibrometer observed the post-impact velocity of the particles. The material properties of the particles and simulation parameters can be seen in Table 4 [89].

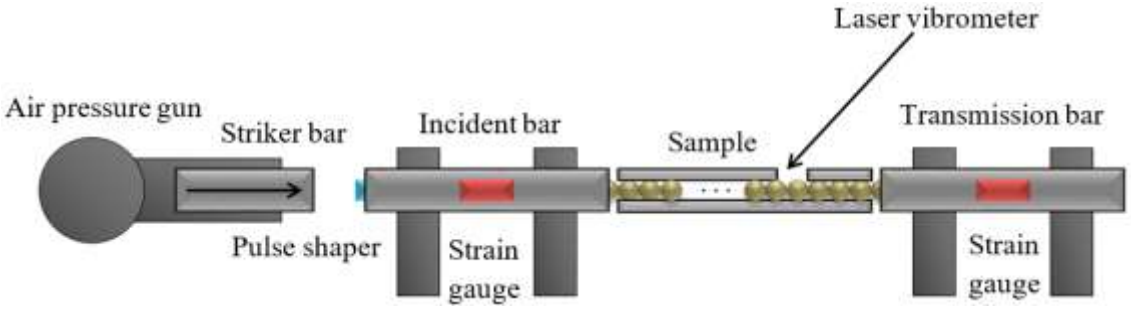

Fig.15 The experimental setup of Hopkinson incident bar [88]

Table 4 Simulation parameters

Parameters	Value
Young's modulus	200 GPa
Poisson ratio	0.307
Yield strength	940 MPa
Coefficient of restitution	0.11
Contact parameter ε	19
Contact parameter Ψ	3.0

The hysteresis damping coefficients between all the spheres are assumed as the damping factor between the first two spheres with initial impact velocity. The impact velocity of the striker bar is assumed as 13 m/s. The contact deformation between the particles is prone to exceed the critical elastic deformation 7.4292E-7 m, which leads to the elastoplastic contact phase being activated during impact behavior. In Fig .16, the post-impact velocity of the 40^{th} particle is measured by the laser vibrometer, which corresponds to the black dash line [88]. The same impact velocity is calculated by the Ma-Liu model, which is represented by the blue dash line. The Ma-Liu model can produce a solution that keeps consistent with the experimental data [89]. Similarly, the post-impact velocity of the 40^{th} particle is also to be obtained using the proposed dashpot model, which also coincides with the experimental data. In this investigation, the elastoplastic deformation is inevitable under high impact velocity. However, the existing dashpot models are not suited for calculating the elastoplastic impact behavior because the Hertz contact stiffness overestimates the contact stiffness in the elastoplastic contact phase [68]. Moreover, although both the proposed dashpot and Ma-Liu models can obtain a rational solution regarding the Hopkinson incident bar, their discrepancy is significant. Because the hysteresis damping factor in the proposed dashpot model can uniform the energy dissipation on the hysteresis loop (blue line) during the whole collision process in Fig. 7, however, the Ma-Liu model utilizes the difference between the loading (black dash line) and unloading (red line) paths to represent the energy dissipation in Fig.7. Therefore, the post-impact velocity profile of the 40^{th} particle in Fig. 16 is smoother than the solution obtained using the Ma-Liu model. However, the numerical solution from the new dashpot model is still deviations from the experimental data. There could be three reasons at least: (i) the friction between the particles does not consider in our model assumption; (ii) the effect of the plastic pipe on the motion status of the particles is neglected; (iii) the sampling error in experimental measurement also results in the discrepancy between the numerical solution and experimental data.

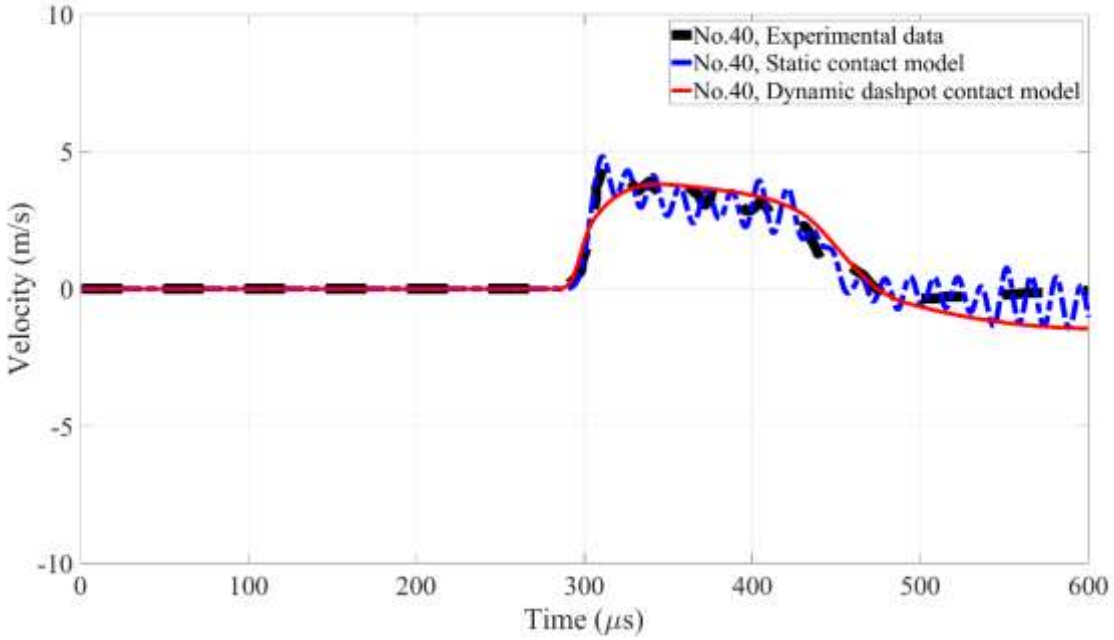

Fig.16 Comparison between the Hopkinson bar's experimental data and the numerical simulations for the post-impact velocity of the 40th particle

7. Conclusions

A comprehensive dashpot model with elastoplastic deformation and hysteresis damping factors is proposed in this work. Since a complete contact process under relative high-speed and large load includes the pure elastic, elastoplastic, and full plastic phases in a sequence, the proposed dashpot model embraces two different contact scenarios. In the elastic phase, the impact behavior is treated as a nonlinear vibration system; a nonlinear hysteresis damping factor is derived by approximately solving this nonlinear system. When the contact comes into the elastoplastic or the plastic phase, the impact behavior is treated as a linear vibration system, since the relationship between the force and deformation is linear from the Ma-Liu model. A linear hysteresis damping factor can be obtained from the linear system. Therefore, a nonlinear dashpot model in the elastic phase is formulated by a nonlinear hysteresis damping factor associated with the Hertz contact stiffness based on the spring-dashpot model; likewise, a linear dashpot model in the elastoplastic or plastic phase is proposed by a linear hysteresis damping factor in conjunction with the linearized elastoplastic contact stiffness. Eventually, a comprehensive dashpot model consists of the elastic dashpot model and elastoplastic dashpot model.

In the elastic phase, the new nonlinear dashpot model is more accurate than the existing dashpot models; in addition, it compensates for the deficiency of the static elastoplastic model by a nonlinear hysteresis damping factor representing the energy dissipation caused by the seismic waves. When the contact deformation surpasses the critical elastic deformation, the new dashpot model can describe that the impact behavior simultaneously undergoes the nonlinear elastic and linear elastoplastic or plastic phases. Compared to the available dashpot models, the new dashpot model can maintain the Ma-Liu model overall when evaluating the elastoplastic impact behavior and accurately calculate the maximum contact force, because the Hertz contact stiffness overestimates the contact stiffness in the elastoplastic phase. Compared to the static elastoplastic model, the new dashpot model simplifies the calculation process of the elastoplastic impact behavior, since it does not need to identify that the contact is in the

compression or the recovery phase. Moreover, it also does not need to save the maximum and residual deformations in each collision for the following impact behaviors, especially for multi-compression and multi-impact scenarios.

The effect of the elastoplastic deformation on the dynamic responses of the slider-crank mechanism with a clearance joint was studied by using the new dashpot model. When the contact behavior in the clearance joint happened within the elastic contact scope, the slider displacement was not sensitive to the contact event. The contact force arisen from the impact behavior resulted in the slider acceleration having a significantly nonlinear vibration, which means that the elastic contact between the clearance joint elements cannot be neglected. However, when the initial impact velocity increases and the contact material has a small yield strength, the elastoplastic deformation seriously affects the slider displacement. The simulation shows that the elastoplastic deformation must be considered in multibody systems. Moreover, the Hopkinson incident bar was treated as a numerical example to check its reasonability under a relatively high impact velocity. The simulation results exhibit that the proposed dashpot model can produce a rational solution to be consistent with the experimental data and the Ma-Liu model, which proves the effectiveness of the proposed dashpot model. Thereby, this new dashpot model provides a new and convenient approach for the dynamic prediction of the elastoplastic impact event in multibody systems.

Acknowledgments:

This work is supported by the National Natural Science Foundation of China (Grant NO. 11932001, NO.12172004, NO. 12111530108, NO.51975449), and the Royal Society under (Grant NO. IEC/NSFC/201059).

References

[1] H. Safaeifar, A. Farshidianfar, A new model of the contact force for the collision between two solid bodies, Multibody Syst. Dyn. (2020). https://doi.org/10.1007/s11044-020-09732-2.

[2] Y. Pan, Y. Sun, C. Min, Z. Li, P. Gardoni, Maneuver-based deep learning parameter identification of vehicle suspensions subjected to performance degradation, Veh. Syst. Dyn. (2022). https://doi.org/10.1080/00423114.2022.2084424.

[3] X. Nie, C. Min, Y. Pan, K. Li, Z. Li, Deep-Neural-Network-Based Modelling of Longitudinal-Lateral Dynamics to Predict the Vehicle States for Autonomous Driving, Sensors. 22 (2022) 1–16. https://doi.org/10.3390/s22052013.

[4] D. Ma, C. Liu, Contact Law and Coefficient of Restitution in Elastoplastic Spheres, J. Appl. Mech. 82 (2015) 1–9. https://doi.org/10.1115/1.4031483.

[5] M. MacHado, P. Moreira, P. Flores, H.M. Lankarani, Compliant contact force models in multibody dynamics: Evolution of the Hertz contact theory, Mech. Mach. Theory. 53 (2012) 99–121. https://doi.org/10.1016/j.mechmachtheory.2012.02.010.

[6] A. Banerjee, A. Chanda, R. Das, Historical Origin and Recent Development on Normal Directional Impact Models for Rigid Body Contact Simulation: A Critical Review, Arch. Comput. Methods Eng. 24 (2017) 397–422. https://doi.org/10.1007/s11831-016-9164-5.

[7] I. Etsion, Y. Kligerman, Y. Kadin, Unloading of an elastic-plastic loaded spherical contact, Int. J. Solids Struct. 42 (2005) 3716–3729. https://doi.org/10.1016/j.ijsolstr.2004.12.006.

[8] R.L. Jackson, I. Green, D.B. Marghitu, Predicting the coefficient of restitution of impacting elastic-perfectly plastic spheres, Nonlinear Dyn. 60 (2010) 217–229.

https://doi.org/10.1007/s11071-009-9591-z.
[9] A.S. Yigit, A.P. Christoforou, M.A. Majeed, A nonlinear visco-elastoplastic impact model and the coefficient of restitution, Nonlinear Dyn. 66 (2011) 509–521. https://doi.org/10.1007/s11071-010-9929-6.
[10] W. Peng, B. Bhushan, Three-dimensional contact analysis of layered elastic/plastic solids with rough surfaces, Wear. 249 (2001) 741–760. https://doi.org/10.1016/S0043-1648(01)00692-5.
[11] E.R. Kral, K. Komvopoulos, D.B. Bogy, Elastic-plastic finite element analysis of repeated indentation of a half-space by a rigid sphere, J. Appl. Mech. Trans. ASME. 60 (1993) 829–841. https://doi.org/10.1115/1.2900991.
[12] Y. Zhao, D.M. Marietta, L. Chang, An Asperity Microcontact Model Incorporating the Transition From Elastic Deformation to Fully Plastic Flow, J. Tribol. 122 (2000) 479–480. https://doi.org/10.1115/1.555389.
[13] E. Corral, R.G. Moreno, M.J.G. García, C. Castejón, Nonlinear phenomena of contact in multibody systems dynamics: a review, Nonlinear Dyn. 104 (2021) 1269–1295. https://doi.org/10.1007/s11071-021-06344-z.
[14] J. Zhang, W. Li, L. Zhao, G. He, A continuous contact force model for impact analysis in multibody dynamics, Mech. Mach. Theory. 153 (2020). https://doi.org/10.1016/j.mechmachtheory.2020.103946.
[15] Dwaikat M. M. S., C. Spitas, V. Spitas, A non-linear model for elastic hysteresis in the time domain: Implementation for multiple degrees of freedom, Proc. Inst. Mech. Eng. Part C J. Mech. Eng. Sci. 235 (2021) 4612–4624.
[16] R.L. Jackson, I. Green, A finite element study of elasto-plastic hemispherical contact against a rigid flat, J. Tribol. 127 (2005) 343–354. https://doi.org/10.1115/1.1866166.
[17] W.J. Stronge, A.R. Sofi, B. Ravani, Computing the composite coefficient of restitution for inelastic impact of dissimilar bodies, Int. J. Impact Eng. 133 (2019) 103333. https://doi.org/10.1016/j.ijimpeng.2019.103333.
[18] A.S. Carvalho, J.M. Martins, Exact restitution and generalizations for the Hunt–Crossley contact model, Mech. Mach. Theory. 139 (2019) 174–194. https://doi.org/10.1016/j.mechmachtheory.2019.03.028.
[19] S. Hu, X. Guo, A dissipative contact force model for impact analysis in multibody dynamics, Multibody Syst Dyn. 35 (2015) 131–151. https://doi.org/10.1007/s11044-015-9453-z.
[20] P. Flores, M. MacHado, M.T. Silva, J.M. Martins, On the continuous contact force models for soft materials in multibody dynamics, Multibody Syst. Dyn. 25 (2011) 357–375. https://doi.org/10.1007/s11044-010-9237-4.
[21] R.G. Herbert, D.C. McWhannell, Shape and Frequency Composition of Pulses From an Impact Pair, J. Eng. Ind. (1977) 513–518.
[22] G. Kuwabara, K. Kono, Restitution Coefficient in a Collision between Two Spheres, Jpn. J. Appl. Phys. 26 (1987) 1230–1233.
[23] T.W. Lee, A.C. Wang, On the dynamics of intermittent-motion mechanisms. Part 1: dynamic model and response., J. Mech. Transm. Autom. Des. 105 (1983) 534–540.
[24] M. Gharib, Y. Hurmuzlu, A New Contact Force Model for Low Coefficient of Restitution Impact, J. Appl. Meclianics. 79 (2012) 1–6. https://doi.org/10.1115/1.4006494.
[25] H.M. Lankarani, P.E. Nikravesh, Continuous contact force models for impact analysis in multibody systems, Nonlinear Dyn. 5 (1994) 193–207. https://doi.org/10.1007/BF00045676.
[26] K. Hunt, E. Crossley, Coefficient of restitution interpreted as damping in vibroimpact, J. Appl. Mech. 42 (1975) 440–445.

[27] H. Minamoto, S. Kawamura, Moderately high speed impact of two identical spheres, Int. J. Impact Eng. 38 (2011) 123–129. https://doi.org/10.1016/j.ijimpeng.2010.09.005.
[28] W.R. Chang, F.F. Ling, Normal impact model of rough surfaces, J. Tribol. 114 (1992) 439–447. https://doi.org/10.1115/1.2920903.
[29] C.Y. Wu, L. yuan Li, C. Thornton, Rebound behaviour of spheres for plastic impacts, Int. J. Impact Eng. 28 (2003) 929–946. https://doi.org/10.1016/S0734-743X(03)00014-9.
[30] L. He, Y. Pan, Y. He, Z. Li, G. Królczyk, H. Du, Control strategy for vibration suppression of a vehicle multibody system on a bumpy road, Mech. Mach. Theory. 174 (2022) 104891. https://doi.org/10.1016/j.mechmachtheory.2022.104891.
[31] M.R. Brake, P.L. Reu, D.J. VanGoethem, M. V. Bejarano, A. Sumali, Experimental validation of an elastic-plastic contact model, ASME 2011 Int. Mech. Eng. Congr. Expo. IMECE 2011. 7 (2011) 733–744. https://doi.org/10.1115/imece2011-65736.
[32] G. Weir, S. Tallon, The coefficient of restitution for normal incident, low velocity particle impacts, Chem. Eng. Sci. 60 (2005) 3637–3647. https://doi.org/10.1016/j.ces.2005.01.040.
[33] Q. Peng, X. Ye, H. Wu, X. Liu, Y.G. Wei, Effect of plasticity on dynamic impact in a journal-bearing system: A planar case, Mech. Mach. Theory. 154 (2020). https://doi.org/10.1016/j.mechmachtheory.2020.104034.
[34] A.H. Kharaz, D.A. Gorham, A study of the restitution coefficient in elastic-plastic impact, Philos. Mag. Lett. 80 (2000) 549–559. https://doi.org/10.1080/09500830050110486.
[35] H. Minamoto, S. Kawamura, Effects of material strain rate sensitivity in low speed impact between two identical spheres, Int. J. Impact Eng. 36 (2009) 680–686. https://doi.org/10.1016/j.ijimpeng.2008.10.001.
[36] C.X. Wong, M.C. Daniel, J.A. Rongong, Energy dissipation prediction of particle dampers, J. Sound Vib. 319 (2009) 91–118. https://doi.org/10.1016/j.jsv.2008.06.027.
[37] W.R. Chang, I. Etsion, D.B. Bogy, An elastic-plastic model for the contact of rough surfaces, J. Tribol. 109 (1987) 257–263. https://doi.org/10.1115/1.3261348.
[38] G. Wang, M.G.R. Faes, F. Cheng, T. Shi, P. Gao, Extension of dashpot model with elastoplastic deformation and rough surface in impact behavior, Chaos, Solitons and Fractals. 162 (2022) 112402. https://doi.org/10.1016/j.chaos.2022.112402.
[39] K. L. Johnson, Contact Mechanics, Cambridge University Press, Cambridge, 1985.
[40] G. Wang, L. Wang, Y. Yuan, Investigation on dynamics performance of multibody system with rough surface, Appl. Math. Model. 104 (2022) 358–372. https://doi.org/10.1016/j.apm.2021.12.012.
[41] W.J. Stronge, Contact Problems for Elasto-Plastic Impact in Multi-Body Systems, in: Impacts Mech. Syst., 2000: pp. 189–234. https://doi.org/10.1007/3-540-45501-9_4.
[42] C. Thornton, Coefficient of Restitution for Collinear Collisions of Elastic- Perfectly Plastic Spheres, J. Appl. Mech. 64 (1997) 383–386.
[43] Y. Du, S. Wang, Energy dissipation in normal elastoplastic impact between two spheres, J. Appl. Mech. 76 (2009) 1–8. https://doi.org/10.1115/1.3130801.
[44] L. Vu-Quoc, X. Zhang, L. Laesburg, A normal force-Displacement model for contacting spheres accounting for plastic deformation: Force-Driven formulation, J. Appl. Mech. 67 (2000) 363–371. https://doi.org/10.1115/1.1305334.
[45] P. Zhao, J. Liu, Y. Li, C. Wu, A spring-damping contact force model considering normal friction for impact analysis, Nonlinear Dyn. 105 (2021) 1437–1457. https://doi.org/10.1007/s11071-021-06660-4.
[46] S.D. Mesarovic, N.A. Fleck, Frictionless indentation of dissimilar elastic-plastic spheres, Int.

J. Solids Struct. 37 (2000) 7071–7091. https://doi.org/10.1016/S0020-7683(99)00328-5.
[47] A.E. Giannakopoulos, Strength analysis of spherical indentation of piezoelectric materials, J. Appl. Mech. Trans. ASME. 67 (2000) 409–416. https://doi.org/10.1115/1.1304913.
[48] Z.H. Jiang, Z.J. Liang, D.W. Zhou, Y.J. Deng, Dissipative properties for a ball bouncing on a vertically vibrating plate, Phys. A Stat. Mech. Its Appl. 548 (2020) 123875. https://doi.org/10.1016/j.physa.2019.123875.
[49] M.R. Brake, An analytical elastic-perfectly plastic contact model, Int. J. Solids Struct. 49 (2012) 3129–3141. https://doi.org/10.1016/j.ijsolstr.2012.06.013.
[50] G. Wang, C. Liu, Further investigation on improved viscoelastic contact force model extended based on hertz's law in multibody system, Mech. Mach. Theory. 153 (2020) 1–24. https://doi.org/10.1016/j.mechmachtheory.2020.103986.
[51] J. Alves, N. Peixinho, M.T. Da Silva, P. Flores, H.M. Lankarani, A comparative study of the viscoelastic constitutive models for frictionless contact interfaces in solids, Mech. Mach. Theory. 85 (2015) 172–188. https://doi.org/10.1016/j.mechmachtheory.2014.11.020.
[52] P. Flores, Contact mechanics for dynamical systems: a comprehensive review, Multibody Syst. Dyn. 54 (2022) 127–177. https://doi.org/10.1007/s11044-021-09803-y.
[53] M. Rodrigues da Silva, F. Marques, M. Tavares da Silva, P. Flores, A compendium of contact force models inspired by Hunt and Crossley's cornerstone work, Mech. Mach. Theory. 167 (2022) 104501. https://doi.org/10.1016/j.mechmachtheory.2021.104501.
[54] L. Vu-Quoc, X. Zhang, An elastoplastic contact force-displacement model in the normal direction: Displacement-driven version, Proc. R. Soc. A Math. Phys. Eng. Sci. 455 (1999) 4013–4044. https://doi.org/10.1098/rspa.1999.0488.
[55] J. Ma, S. Dong, G. Chen, P. Peng, L. Qian, A data-driven normal contact force model based on artificial neural network for complex contacting surfaces, Mech. Syst. Signal Process. 156 (2021) 107612. https://doi.org/10.1016/j.ymssp.2021.107612.
[56] P. Ravn, A Continuous Analysis Method for Planar Multibody Systems with Joint Clearance, Multibody Syst. Dyn. 2 (1998) 1–24. https://doi.org/10.1023/A:1009759826529.
[57] J. Chung, G.M. Hulbert, A time integration algorithm for structural dynamics with improved numerical dissipation: The generalized-α method, J. Appl. Mech. Trans. ASME. 60 (1993) 371–375. https://doi.org/10.1115/1.2900803.
[58] H.M. Lankarani, P.E. Nikravesh, A contact force model with hysteresis damping for impact analysis of multibody systems, J. Mech. Des. Trans. ASME. 112 (1990) 369–376. https://doi.org/10.1115/1.2912617.
[59] Y. Gonthier, J. Mcphee, C. Lange, J. Piedbœuf, A Regularized Contact Model with Asymmetric Damping and Dwell-Time Dependent Friction, Multibody Syst. Dyn. 11 (2004) 209–233.
[60] P. Flores, J. Ambrósio, On the contact detection for contact-impact analysis in multibody systems, Multibody Syst. Dyn. 24 (2010) 103–122. https://doi.org/10.1007/s11044-010-9209-8.
[61] A. He, J.S. Wettlaufer, Hertz beyond belief, Soft Matter. 10 (2014) 2264–2269. https://doi.org/10.1039/c3sm53063a.
[62] S. Bing, J. Ye, Dynamic analysis of the reheat-stop-valve mechanism with revolute clearance joint in consideration of thermal effect, Mech. Mach. Theory. 43 (2008) 1625–1638. https://doi.org/10.1016/j.mechmachtheory.2007.12.004.
[63] L.Y. Li, C.Y. Wu, C. Thornton, A theoretical model for the contact of elastoplastic bodies, Proc. Inst. Mech. Eng. Part C J. Mech. Eng. Sci. 216 (2002) 421–431.

https://doi.org/10.1243/0954406021525214.
[64] J. Coaplen, W.J. Stronge, B. Ravani, Work equivalent composite coefficient of restitution, Int. J. Impact Eng. 30 (2004) 581–591. https://doi.org/10.1016/j.ijimpeng.2003.10.038.
[65] T.J.R. Hughes, R.L. Taylor, J.L. Sackman, A. Curnier, W. Kanoknukulchai, A finite element method for a class of contact-impact problems, Comput. Methods Appl. Mech. Eng. 8 (1976) 249–276. https://doi.org/10.1016/0045-7825(76)90018-9.
[66] P. Lan, K. Li, Z. Yu, Computer implementation of piecewise cable element based on the absolute nodal coordinate formulation and its application in wire modeling, Acta Mech. 230 (2019) 1145–1158. https://doi.org/10.1007/s00707-018-2332-y.
[67] G. Wang, C. Liu, Y. Liu, Energy Dissipation Analysis for Elastoplastic Contact and Dynamic Dashpot Models, Int. J. Mech. Sci. 221 (2022) 107214. https://doi.org/10.1016/j.ijmecsci.2022.107214.
[68] G. Wang, C. Liu, Nonlinear wave in granular systems based on elastoplastic dashpot model, Int. J. Mech. Syst. Dyn. 1 (2021) 132–142. https://doi.org/10.1002/msd2.12008.
[69] J. Ma, G. Chen, L. Ji, L. Qian, S. Dong, A general methodology to establish the contact force model for complex contacting surfaces, Mech. Syst. Signal Process. 140 (2020) 106678. https://doi.org/10.1016/j.ymssp.2020.106678.
[70] J. Hu, F. Gao, X. Liu, An elasto-plastic contact model for conformal contacts between cylinders, Proc IMechE Part JJ Eng. Tribol. (2019) 1–9. https://doi.org/10.1177/1350650119896461.
[71] J. Zhang, W. Li, L. Zhao, G. He, A continuous contact force model for impact analysis in multibody dynamics, Mech. Mach. Theory. 153 (2020) 103946. https://doi.org/10.1016/j.mechmachtheory.2020.103946.
[72] K. Hashemnia, Experimental study of the effect of temperature on the coefficient of restitution of steel balls impact to some industrial metal sheets at elevated temperatures, Powder Technol. 368 (2020) 170–177. https://doi.org/10.1016/j.powtec.2020.04.053.
[73] P. Ranganath Nayak, Random process model of rough surfaces, J. Tribol. 93 (1971) 398–407. https://doi.org/10.1115/1.3451608.
[74] K. Hanley, F. Collins, K. Cronin, E. Byrne, K. Moran, D. Brabazon, Simulation of the impact response of a sliotar core with linear and non-linear contact models, Int. J. Impact Eng. 50 (2012) 113–122. https://doi.org/10.1016/j.ijimpeng.2012.06.006.
[75] D.W. Marhefka, D.E. Orin, Simulation of contact using a nonlinear damping model, Proc. - IEEE Int. Conf. Robot. Autom. 2 (1996) 1662–1668. https://doi.org/10.1109/robot.1996.506951.
[76] C. Spitas, M.M.S. Dwaikat, V. Spitas, Non-linear modelling of elastic hysteretic damping in the time domain, Arch. Mech. 72 (2020) 323–353. https://doi.org/10.24423/aom.3536.
[77] C. Spitas, A continuous piecewise internal friction model of hysteresis for use in dynamical simulations, J. Sound Vib. 324 (2009) 297–316. https://doi.org/10.1016/j.jsv.2009.02.006.
[78] F. Di Puccio, L. Mattei, A novel approach to the estimation and application of the wear coefficient of metal-on-metal hip implants, Tribol. Int. 83 (2015) 69–76. https://doi.org/10.1016/j.triboint.2014.10.023.
[79] Q. Tian, P. Flores, H.M. Lankarani, A comprehensive survey of the analytical, numerical and experimental methodologies for dynamics of multibody mechanical systems with clearance or imperfect joints, Mech. Mach. Theory. 122 (2018) 1–57. https://doi.org/10.1016/j.mechmachtheory.2017.12.002.
[80] J. Ma, L. Qian, Modeling and simulation of planar multibody systems considering multiple

revolute clearance joints, Nonlinear Dyn. 90 (2017) 1907–1940. https://doi.org/10.1007/s11071-017-3771-z.
[81] J. Ma, G. Chen, L. Ji, L. Qian, S. Dong, A general methodology to establish the contact force model for complex contacting surfaces, Mech. Syst. Signal Process. 140 (2020) 106678. https://doi.org/10.1016/j.ymssp.2020.106678.
[82] P. Flores, C.S. Koshy, H.M. Lankarani, J. Ambrósio, J.C.P. Claro, Numerical and experimental investigation on multibody systems with revolute clearance joints, Nonlinear Dyn. 65 (2011) 383–398. https://doi.org/10.1007/s11071-010-9899-8.
[83] P. Chen, J.Y. Liu, G.C. Lu, A new subregion mesh method for the investigation of the elastic-plastic impact in flexible multibody systems, Acta Mech. Sin. 33 (2017) 189–199. https://doi.org/10.1007/s10409-016-0603-1.
[84] F. Marques, P. Flores, J.C.P. Claro, H.M. Lankarani, Modeling and analysis of friction including rolling effects in multibody dynamics: a review, Multibody Syst. Dyn. 45 (2019) 223–244. https://doi.org/10.1007/s11044-018-09640-6.
[85] A.T. Guide, L.D. Problem, B.Y. Model, T. Your, F. Prototype, V. Results, A. Physical, T. Data, R.Y. Design, I.Y. Design, O.Y. Design, D. Process, Getting Started Using ADAMS / View, (n.d.).
[86] N. Song, H. Peng, X. Xu, G. Wang, Modeling and simulation of a planar rigid multibody system with multiple revolute clearance joints based on variational inequality, Mech. Mach. Theory. 154 (2020). https://doi.org/10.1016/j.mechmachtheory.2020.104053.
[87] F. Isaac, F. Marques, N. Dourado, P. Flores, A finite element model of a 3D dry revolute joint incorporated in a multibody dynamic analysis, Multibody Syst. Dyn. 45 (2019) 293–313. https://doi.org/10.1007/s11044-018-09659-9.
[88] H.A. Burgoyne, C. Daraio, Elastic-plastic wave propagation in uniform and periodic granular chains, J. Appl. Mech. Trans. ASME. 82 (2015) 1–10. https://doi.org/10.1115/1.4030458.
[89] Y. Feng, W. Kang, D. Ma, C. Liu, Multiple Impacts and Multiple-Compression Process in the Dynamics of Granular Chains, J. Comput. Nonlinear Dyn. 14 (2019). https://doi.org/10.1115/1.4044584.